

Development of Graphene based Cobalt-ferrites nanocomposites for microwave shielding

A Thesis submitted to Department of Materials Engineering, School of Chemical and Materials Engineering (SCME), NUST, in partial fulfillment of the requirements for the degree of

MASTER OF SCIENCE (MS)

In

MATERIALS AND SURFACE ENGINEERING



By

MUHAMMAD SIYAR

2011-NUST-MS Ph.D-MS-E-17

Supervised By

Meritorious Prof. Dr Asghari Maqsood.SI.

**SCHOOL OF CHEMICAL AND MATERIALS ENGINEERING (SCME), NATIONAL
UNIVERSITY OF SCIENCES AND TECHNOLOGY (NUST), H-12, ISLAMABAD,
PAKISTAN**



CERTIFICATE

This is to certify that the work in this dissertation has been carried out by Muhammad Siyar and completed under my supervision at School of Chemical and Materials Engineering, National University of Science and Technology, Islamabad, Pakistan.

Meritorious Prof. Dr Asghari Maqsood.SI

Supervisor

*Centre for Emerging Sciences, Engineering & Technology,
(CESET), Islamabad, Pakistan.*

Submitted through

Prof. Dr. Mohammad Mujahid

Dean/ Principal

*School of Chemical and Materials Engineering,
National University of Science and Technology,
Islamabad, Pakistan.*

**DEDICATED TO
MY PARENTS, BROTHERS, TEACHERS & FRIENDS**

ACKNOWLEDGEMENT

Scientists explore the world as is...
Engineers create the world that has never
been with Allah's will...

In the name of ALLAH, the Most Gracious and the Most Merciful. All praises to ALLAH for the strength and His blessing in successful completion of this study. I offer my strong gratitude to the last Prophet MUHAMMAD (S.A.W), who is the great leader and guide us towards humanity, peace and justice.

I would like to gratefully and sincerely thank Dr. Asghari maqsood for her guidance, understanding, patience, and most importantly her support, She encouraged me to not only grow as an experimentalist and a chemist but also as an independent thinker.

Besides my advisor, I would like to thank Dr Muhammad mujahid Dean and principal of SCME (NUST), for his kind support and help during my characterization and synthesis. He always supported me to operate instrument myself and that's why satisfactory results were achieved which may other wise very difficult.

I want to give gratitude to Dr Muhammad Shaid, HOD material department for his encouragement and full support at every stage of my entire graduation. He tried his best to solve any problem we faced during my studies and provide us a full equipped platform for our research.

I also feel honor to acknowledge Dr. Arshad Head of Chemical Engineering Department for providing the laboratory facilities.

Moreover I would like to thanks my GEC committee members Dr. Iftikhar Hussain Gul, Dr Habib Nasir and specially Dr. Amir Habib who inspired me toward nanotechnology and motivated me that I worked on graphene synthesis.

I express my special thanks to MRL (UOP) and physics department UET Lahore where they provided me lab facility to perform some characterization.

I acknowledge School of Chemical and Materials Engineering (SCME), NUST, Pakistan, for the technical and financial assistance provided during my study and research work. I also acknowledge PSF, project 147 (Pakistan Science Foundation) for providing funding to TTL laboratory at SCME (NUST), where I performed various tests of my samples.

My bundle of thanks to all the faculty members, non-teaching staff, my fellow students, Friends and seniors who helped me at the various stages of my graduation.

Last but not the least I will like to thank my Parents, and brothers without their support this work would have never been accomplished.

MUHAMMAD SIYAR

Abstract

In this study we developed graphene based cobalt ferrites composites by in situ co-precipitation route. Four samples were prepared with 0%, 0.1%, 0.5% and 1% graphene sheets to cobalt ferrites. The samples were characterized by XRD, and FTIR, while SEM was used to observe the hybrid structure of embed graphene sheets in cobalt ferrites. SEM confirms the successful adhesion of cobalt ferrites particles (10-20 nm) on graphene nano sheets, which are dispersed in metal oxide matrix.

Microwave absorbing capacity of these samples was studied by Agilent network analyzer in low frequency band of microwave (1MHz to 2 GHz), Results reveals that graphene incorporation not only improved the absorption capacity of cobalt ferrites(13dB-17d), but also widened its maximum absorption peak. This change was supposed to be due to inhomogeneity and combine effects of electric (graphene), and magnetic dielectric nature (cobalt ferrites).

Further mechanical characterizations reveal that our composites samples have higher flexural strength (19.92 MPa for 1 % loading) and improved toughness (>6000 J/mm²) compare to pure cobalt ferrites (10.28 MPa, 1000 J/mm²).

Table of contents

CERTIFICATE	3
DEDICATION	4
ACKNOWLEDGEMENT	5
Abstract.....	7
Table of contents.....	8
CHAPTER 1	12
1.1 Background	12
1.2 Objectives.....	13
1.3 Outlines.....	13
CHAPTER 2	16
2. Introduction to Graphene	17
2.1 Carbon and its Derivatives.....	17
2.1.1 Graphene	18
2.1.1.1 History of Graphene	18
2.1.1.2 Synthesis of Graphene.....	19
2.1.1.2.1 Bottom up Approach	19
2.1.1.2.1.1 Chemical Vapor Deposition (CVD).....	19
2.1.1.2.1.2 Epitaxial Growth On SiC	20
2.1.1.2.2 Top-down Approach.....	20
2.1.1.2.2.1 Direct Exfoliation of Graphite	20
2.1.1.2.2.2 Graphene Oxide	20
2.1.1.2.2.3 Electrochemical Route	21
2.1.1.3 Properties and Applications of Graphene.....	21
2.1.1.3.1 Graphene Electronics	21
2.1.1.3.2 Graphene Transistors	21
2.1.1.3.3 Graphene Optoelectronics.....	22
2.1.1.3.4 Graphene Sensors	22
CHAPTER 3	27
3.1 Introduction to Ferrites.....	28
3.2 Structure of Ferrites.....	29
3.3 Synthesis Routes of Ferrites	30

3.4 Properties and Applications.....	31
CHAPTER 4	35
4.1 Microwave Shielding, Problems and Solutions.....	36
4.2 Use of Microwave.....	36
4.3 Issues Caused By Microwave	37
4.3.1 Biological Issue	37
4.3.2 Electromagnetic Noises.....	38
4.4 Microwave Shielding.....	39
4.4.1 Dielectric Material Absorber.....	39
4.4.1 Resonant Absorbers.....	39
4.4.2 Graded Dielectric Absorbers.....	40
Chapter 5	44
5. Materials and Methods.....	44
5.1 Materials.....	44
5.1.2 Equipment Used	44
5.2 Characterization Techniques	44
5.2.1 XRD.....	45
5.2.2 FTIR Spectroscopy.....	45
5.2.3 Raman Spectroscopy.....	46
5.2.4 SEM Analysis	46
5.2.5 AFM.....	47
5.2.6 Electrical Measurements.....	48
5.2.6.2 Die design.....	49
5.2.7 Mechanical characterizations	49
5.2.7.1 Flexural Strength.....	49
5.2.7.2 Micro Vickers Hardness	49
CHAPTER 6	55
6.1 Lab Work Performed.....	55
6.1.1 Phase 1: optimization of graphene oxide synthesis	55
6.1.1.1 Hummer Method	55
6.1.1.2 Novel Pre-sonication Route	56
6.1.1.3 Hummer Modified Method.....	56
6.1.2 Phase 2: Reduction Methods of GO.....	56
6.1.2.1 Reduction by Hydrazine.....	56

6.1.2.2 Reduction by Sodium Borohydride	56
6.1.2.3 Novel Reduction by Sodium Hydroxide.....	57
6.1.3 Phase 3: In situ Syntheses of Cobalt Ferrites-graphene Composites	57
CHAPTER 7	60
7 Results and Discussion.....	60
7.1 XRD Characterization	60
7.1.2 Reduction of GO	61
7.1.3 Phase Analysis of Composites	61
7.2 FTIR Analysis	62
7.2.1 Functional Group Analysis of GO.....	62
7.2.2 Groups Present in RGO Samples	63
7.2.3 FTIR Analysis of Cobalt Ferrites and its Composites.....	64
7.3 Raman Spectroscopy.....	65
7.3.1 Raman Spectra of GO Samples.....	65
7.4 Size, Morphology and Topography.....	67
7.4.1 SEM and AFM of GO samples.....	67
7.4.2 SEM of RGO Samples.....	72
7.4.3 SEM of Ferrites and its Composites Samples.....	73
7.5 Electrical Characterization.....	74
7.5.1 Real permittivity and Permeability	75
7.5.2 Complex Permittivity and Permeability	76
7.5.3 Microwave Absorption.....	77
7.6 Mechanical Characterization.....	79
7.6.1 Stress versus Strain Behavior	79
7.6.2 Toughness.....	80
7.6.3 Flexural Stregth	81
7.6.4 Vickers Hardness	82
CHAPTER 8	87
8 Conclusion and Recommendations.....	87
8.1 Conclusion	87
8.2 Future Recommendations.....	87

CHAPTER 1

Introduction

1.1 Background

After the discovery of graphene in 2004 by A.K. Geim and K.S. Novoselov [1], Scientist extensively started interest in the study and applications of this important material to cope with modern scientific challenges [2, 3, and 4]. In short span so many educational and industrial organizations put their efforts to explore its properties for useful applications. Individual graphene sheet is thought to be a potential candidate for future electronics such as FETs and flexible displays [5, 6].

Besides pure graphene sheet, functionalized graphene (RGO) which is obtained through chemical synthesis routes by reducing graphene oxide is also equally important due to ease of preparation and application[7,8]. Due to different groups attached with graphene sheet in RGO, its conductivity is not remaining as in pure form but reduces several times [9]. Although the properties of RGO is totally different from single graphene sheet but still having some tremendous properties such as good conductivity high mechanical strength and transparent nature [10, 11]. Peoples are trying to improve the mechanical and electrical properties of other materials by making composites of it with RGO as well as to make devices from pure RGO for different applications [12, 13]. Due to high surface area and sheet like morphology nanoparticles are efficiently dispersed on it to make good adhesion and hence best results can be obtained.

Ferrites are the magnetic mix metal oxides comprising the ferric ions as an essential constituent, while in mineralogy or in metallurgy the term ferrites refer to that material having a cubic crystal structure of spinal mineral[14,15]. The ferrites application has been known from ancient times for multiple centuries. Magnetite or ferrous ferrite is a naturally occurring ferrite. Among all cobalt ferrites is also a promising candidate for medical treatment, electronic circuits telecom and RF applications [16-18]. There are so many efforts have been done to make microwave absorbing materials from ferrites, but such materials are facing obstacles to perform efficiently, due to heavy weight and poor mechanical properties[19,20].

To overcome these problems researchers started to make its composites with different matrix materials and to develop materials for specific area of application [21]. To get flexible and light weight sheets, ferrites are used to mixed with different polymers to improve its mechanical properties but rise the problem of low thermal conductivity and caused heat accumulation in the covered device as well as with in the sheet it self which may led to severe problems and degradation of these absorbing sheets[22,23].

In present work we have prepared cobalt ferrites composites with graphene nanosheet, to overcome the problem stated above.

1.2 Objectives

Aim of this study is to achieve the following goals

1. Efficient synthesis of monolayer graphene oxide for composites application.
2. To reduce graphene oxide and evaluate its electrical and mechanical properties.
3. Synthesis of nano cobalt ferrites and its composites with graphene.
4. To see the effect of graphene loading into ferrites matrix on its electrical and mechanical properties

1.3 Outlines

Chapter 1 of the thesis gives an overview, motivation and scope of the topic. In chapter 2 we summarized some basic introduction to graphene and its derivatives along with its numerous properties and previous work done. Chapter 3 is related to ferrites its structure properties and applications. Chapter 4 comprising of basic microwave study, its uses and challenges. Chapter 5 deals with all the laboratory work done, which includes materials synthesis and optimizations. In chapter 6 we listed the basic working principles and scope of all the characterization tools we used. Finally chapter 7 includes the results and discussions of tested materials individually and in composites form, on the basis of these results a final conclusion is drawn to address the issue discussed in start.

References

1. K. S. Novoselov, A. K. Geim, S. V. Morozov, D. Jiang, Y. Zhang, S. V. Dubonos, I. V. Grigorieva and A. A. Firsov. *Science* 2004; 306: 666.
2. K. S. Novoselov, A. K. Geim, S. V. Morozov, D. Jiang, Y. Zhang, S. V. Dubonos, I. V. Grigorieva, and A. A. Firsov. Electric Field Effect in Atomically Thin Carbon Films. *Science* 2004; 306:666–669.
3. Charlier, J. C. Eklund, P. C. Zhu, J. Ferrari, A. C. Electron and phonon . Their relationship with carbon properties of graphene: The nanotubes. *Top. Appl. Phys* 2008; 111: 673–709.
4. Hwang et al, Graphene as Thin Film Infrared Optoelectronic. *ACS Nano* 2003.
5. C. Navarro, R. Weitz, A. Bittner, M. Scolari, A. Mews, M. Burghard and K. Kern. Electronic transport properties of individual chemically reduced graphene oxide sheet. *Nano Let.* 2007; 7:3499–3503.
6. J. Yao, J. Lin, Y. Dai, G. Ruan, Z. Yan, L. Li, L. Zhong, D. Natelson and J. M. Tour. Highly transparent nonvolatile resistive memory devices from silicon oxide and graphene. *Nature Communications*. 2012; 3: 11-01.
7. K. Moon, J. G. Rodney, S. Ruoff and H. Lee. Reduced graphene oxide by chemical graphitization. *Nature communications* 2010; 1.
8. A. Elzatahry Aboubakr M. Abdullah et al. J. Electrochem Nanocomposite Graphene-Based Material for Fuel Cell Applications. *International Journal of* 2012; 7; 3115 – 3126.
9. A. Elzatahry Aboubakr M. Abdullah et al. J. Electrochem. Nanocomposite Graphene-Based Material for Fuel Cell Applications *International Journal of* 2012; 7; 3115 – 3126.
10. N. Liu et al. One-Step Ionic-Liquid-Assisted Electrochemical Synthesis of Ionic-Liquid Functionalized Graphene Sheets Directly from Graphite. *Adv. Funct Mater* 2008; 18:1518-1525.
11. W. L. Zhi and K. Müllen. Transparent, Conductive Graphene Electrodes for Dye-Sensitized Solar Cells 2007; Revised Manuscript Received November 1
12. Ma Y W, Zhang L R, Li J J, et al. Carbon-nitrogen/graphene composite as metal-free electrocatalyst for the oxygen reduction reaction. *Chin Sci Bull* 2011; 56: 3583–3589.
13. Zhang Q O, He Y Q, Chen X G, et al. Structure and photocatalytic properties of ThO₂-graphene oxide intercalated composite. *Chin Sci Bull* 2013; 56: 331–339.
14. R. Valenzuela, *Magnetic Ceramics*, Cambridge University Press, (1994) London.
15. V. R. K. Murthy and B. Viswanathan. *Ferrite Materials Science and Technology*, Narosa Publishing House (1962), New Delhi.
16. V. Pallai and D.O Shah. *Journal of Magnetism and Magnetic Materials* 1996; 163: 243-248.
17. G. Ranga Mohan a, D. Ravinder a , A.V. Ramana Reddy and B.S. Boyanov . Dielectric properties of polycrystalline mixed nickel–zinc ferrites 1999.

18. W. Eerenstein, N. D. Mathur & J. F. Scott, Multiferroic and magnetoelectric materials, *Nature* 2006; 442:759.
19. E. Manova, D. Paneva, B. Kunev, Cl. Estournès, E. Rivière, K. Tenchev, A. Léaustic and I. Mitov. Mechanochemical synthesis and characterization of nanodimensional iron-cobalt spinel oxides. *Journal of Alloys and Compounds* 2009; 485: 356-361.
20. Z. Zi, Y. Sun, X. Zhu, Z. Yang, J. Dai and W. Song. Synthesis and magnetic properties of CoFe O ferrite nanoparticles. *Journal of Magnetism and Magnetic Materials* 2009; 321: 1251-1255.
21. K. Singh, A. Ohlan, P. Saini, and S. K. Dhawan. *Polym. Adv. Technol* 2008; 19: 229.
22. O. Yavuz, M. K. Ram, and M. Aldissi, *J. Mater. Chem.* 2005; 15: 810.
23. N. E. Kazantseva, J. Vilcakova, and V. Kresalek, *J. Magn. Magn. Mater.* 2004; 269: 30.

CHAPTER 2

Introduction to Graphene

2.1 Carbon and its Derivatives

Carbon is always found almost everywhere. It's in the clothes, food, fuel, air and so many things we use. So carbon is an important element in the universe.

There are four atoms in carbon outer valence shell and can accommodate four more electrons, since each carbon atom may share its valence electrons with four different atoms. Carbon can make bonding with so many other elements and with it also. That's why carbon can form so many different compounds of different size and shape [1]

Carbon is found in their different forms, graphite, diamond, amorphous carbon, and fluorine and carbon nanotubes [2]. Diamond is the hardest and insulator while graphite is slippery and conductive under normal conditions. The difference in the nature of these allotropes is solely due to the way in which these atoms arranged [3].

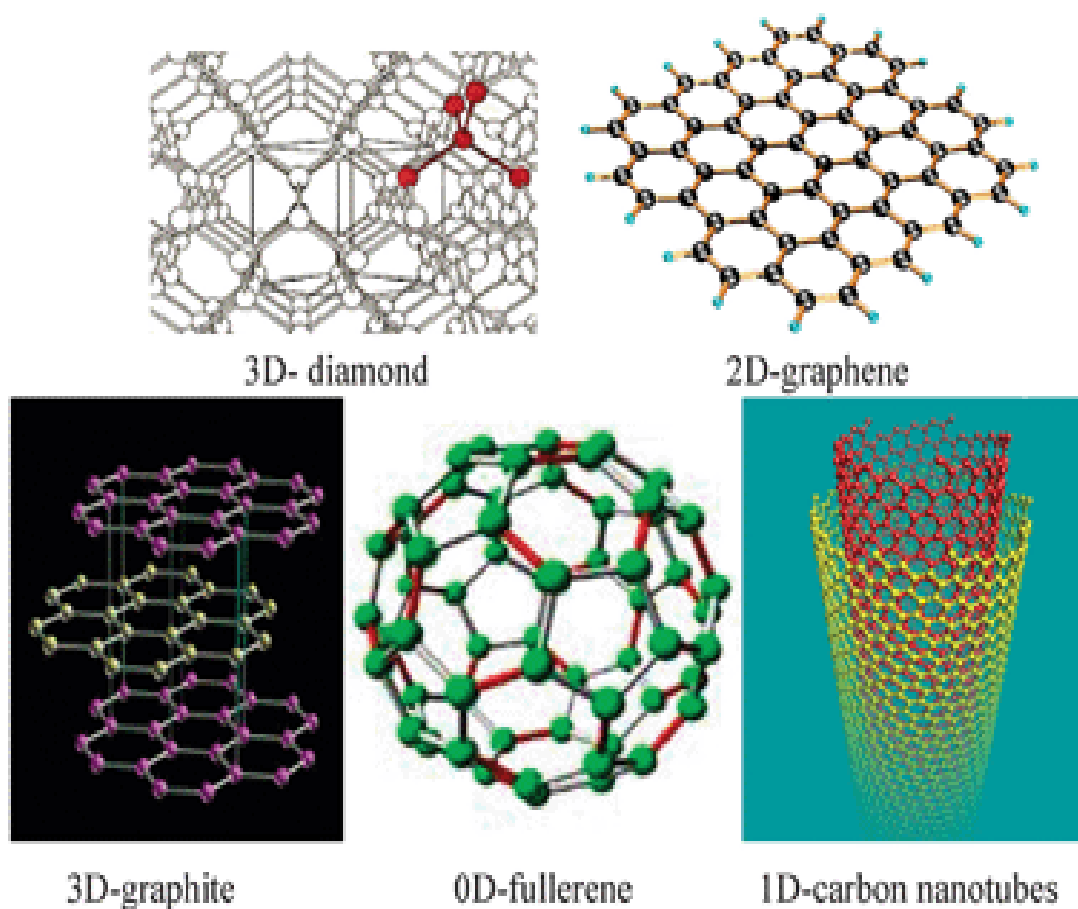


Figure 2.1. Different derivatives of carbon [58]

2.1.1 Graphene

Graphene has 2D layer hexagonal structure of single carbon atoms [4]. The carbon bonds are formed by sp^2 hybridization, the σ -bond between in plane C-C atoms is considered the strongest bond found in materials and the π bond is out-of-plane. Having a network of delocalized electrons is responsible for electron mobility of graphene, and also facilitate the linkage among the planes of graphite or with any substrate that's why graphene sheet is the most strongest and the layers may be covered so easily. Due to this unique bonding structure graphene have magical nature and have exceptional physical properties [5-13]. It has brought stormy revolution in electronics and nanosciences due to its outstanding electrical, mechanical, ballistic transport properties, chemically inert, and the transparent nature [14-18].

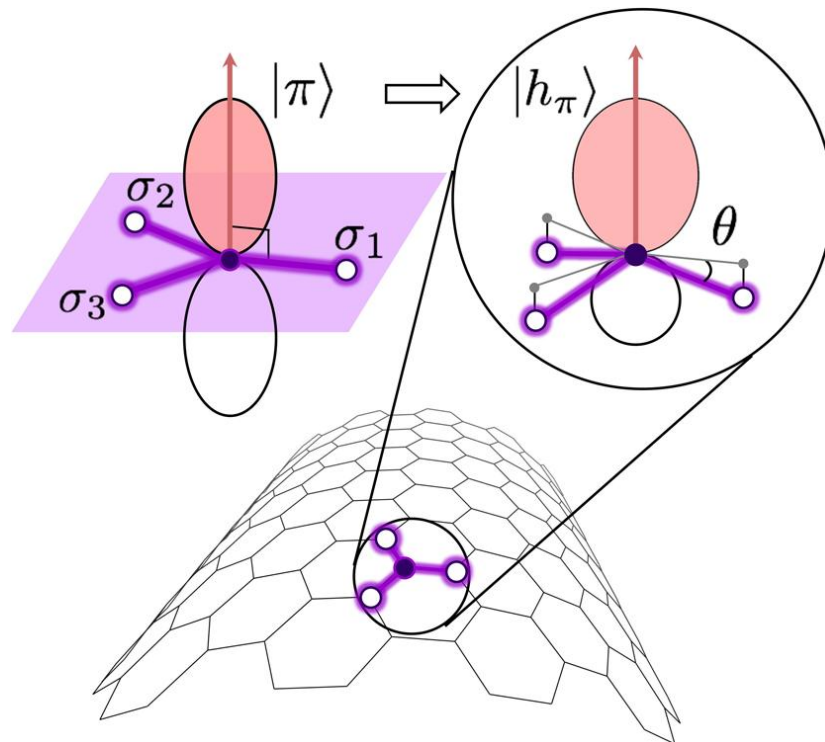


Figure 2. 2. Bonding structure of graphene [17]

2.1.1.1 History of Graphene

The initial attempts were taken by Schafjauertl a German scientist in the 1840s, when he reported the chemical exfoliation of graphite with the help of nitric acids and sulfuric acids separating the carbon lamellae of graphite [19-21]. After that so many experimentations were performed to intercalate the graphite layer by the insertion of small molecule-species like alkali or acid molecule including fluoride salts of

different types, metals like nickel, iron etc, [22–25]. Boehm and co-workers reported in 1962 the successful synthesis of monolayer and few layers reduced graphene oxide by the chemical and thermal reduction of graphite oxide [26].

At the start of 1997 IUPAC formalized that graphene terminology will be discussed in the work comprising of reactions, chemical structures or other characteristic properties of individual graphene flakes [27]. After four years later W. de Heer, synthesized planer graphene sheets through thermal route by heating SiC at 1300 °C and also discussed its physical nature [28].

Finally in 2004 Geim and Novoselov from MIT research lab reported the formation of monolayer and a few layers of graphene sheets through mechanical exfoliation techniques. They haven't only synthesized graphene but also studied its electrical and magnetic properties of it. The Nobel Prize of Physics in 2010 was awarded for this novel discovery to Geim and Novoselov [29-30].

2.1.1.2 Synthesis of Graphene

Number of synthesis routes for monolayer or few layer graphene have been explored so far [31-33]. We may categorize these synthesis routes in two main types, Bottom up approach and top down approach.

2.1.1.2.1 Bottom up Approach

In this synthesis route , graphene is produced by reacting some pure carbon containing precursors , while providing some inert and heated medium as a result of which carbon atoms assemble and bond in the structure of graphene. This is the very effective route for defect free graphene sheets but limited to small area flakes and also very expensive.

2.1.1.2.1.1 Chemical Vapor Deposition (CVD)

For graphene synthesis via CVD, a quartz tube is used as a reactor in a tube furnace. Graphite electrodes are placed at the bottom and the top of the chamber while N₂ and Aragon are used to provide the inert media within the chamber. Different types of metal substrates like copper and aluminum are used for deposition of graphene sheets. Annealing is done up to 1000 °C in the presence of CH₄ and H₂ precursor, followed by rapid cooling to get graphene thin films as referred in the following figure 3.[34].

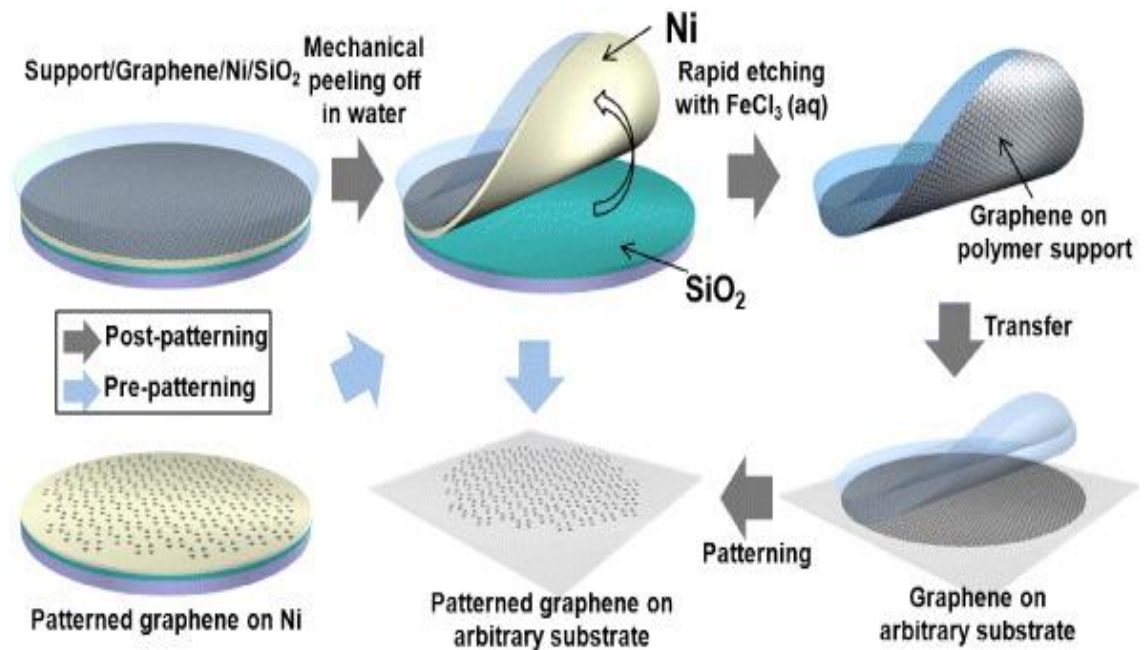


Figure 2. 3. Detail process of CVD synthesis of graphene [61]

2.1.1.2.1.2 Epitaxial Growth On SiC

Here 4-H and 6-H-SiC may be chosen as the depositing substrates for the epitaxial growth of graphene. Hydrogen etching or mechano-chemical polishing are performed to get atomically smooth surface of the substrate. In a quartz tube SiC substrates are annealed in the range of 600 °C to 1000 °C in either UHV or Ar atmosphere under atmospheric pressure. Hence Si sublimation takes place to grow the remaining carbon atoms in the shape of graphene layers [35-36].

2.1.1.2.2 Top-down Approach

In the top down approach, graphene is synthesized by taking bulk graphite or graphite derivatives and then its layers are exfoliated or cleaved until we get mono or a few layers of graphene flakes. Although in such a way we get graphene along with so many structural defects, but are useful route to get large scale graphene especially for composites applications.

2.1.1.2.2.1 Direct Exfoliation of Graphite

Graphite is exfoliated by sonication in the presence of Polyvinylpyrrolidone, Benzene, or N-Methylpyrrolidone, into graphene nano sheets. Through this route monolayer or few layer graphene may be possible but separation of individual graphene flakes is the challenging task. To dissolve these exfoliated flakes chlorosulfonic acid is used but is strong hazardous and hence limit to apply this method commercially [37-38].

2.1.1.2.2.2 Graphene Oxide

Graphene production from reduction of graphene oxide (GO), is the most auspicious way for large scale synthesis. Here pure graphite is first oxidized with the help of strong oxidizing agents like KMnO_4 , KClO_3 and NaNO_3 in the presence of sulfuric acids, Nitric acids or phosphoric acids. Single or multilayer layer graphene oxide sheets are obtained when dispersed in water form a yellowish solution. Reduction of GO by hydrazine, results in reduced graphene sheets (RGO). Due to a large number of defects present in the final product, the application is limited to use only in composites [39-42].

2.1.1.2.3 Electrochemical Route

This is the modern technique developed recently for graphene production. Two high purity graphite electrodes are immersed in an electrolyte bath, having water along with ionic liquid. When static potential is applied across the electrodes, a nod graphite electrode starts corroding and results a black precipitate in the electrolyte cell. After the completion of electrolysis a stable dispersion of graphene nano sheets is achieved, which is filtered and dried to get graphene powder [43].

2.1.1.3 Properties and Applications of Graphene

Some major applications of graphene are listed below.

2.1.1.3.1 Graphene Electronics

Graphene has tremendous electrical and physical properties so scientists hope the solution of modern world challenges through the use of this magical material. It has high charge carrier mobility up to $100\,000\text{ cm}^2/\text{V}\cdot\text{s}$ [44-45], incredible current carrying capacity ($10\,9\text{ Amp}/\text{cm}^2$) [46] extraordinary thermal conductivity reported up to $5000\text{ Wm}^{-1}\text{ K}^{-1}$, along with high strength [47] and transparent nature [48]. Graphene is zero band semiconductors, [49] planar material that's why, seeking a future in modern electronics, to be used in nano electrical circuits as conductive channels, transparent and flexible Liquid Color Display (LCD) and so more.

2.1.1.3.2 Graphene Transistors

If the carriers may induce into the channel of graphene, their electrical transport can be restrained by a gate-injected electric field. When positively biased the electron energy of the gate lessened, while a negative bias raises it. For e_f below the neutral point (e_{nf}) in ambipolar graphene, transport is carried out by holes, while for e_f above e_{nf} electrons are responsible for transport. As gate biasing, the states-density and the carrier density may change the Fermi energy so lead to switching in field effect transistors in graphene (GFETs) [50]. Due to low on/off ratio of 2D graphene, is not guaranteed to be used in digital switches, but its excellent carrier mobility, ultimate strength and stability make it an excellent candidate for radio-frequency transistors (RFTs) and fastest analog systems [51].

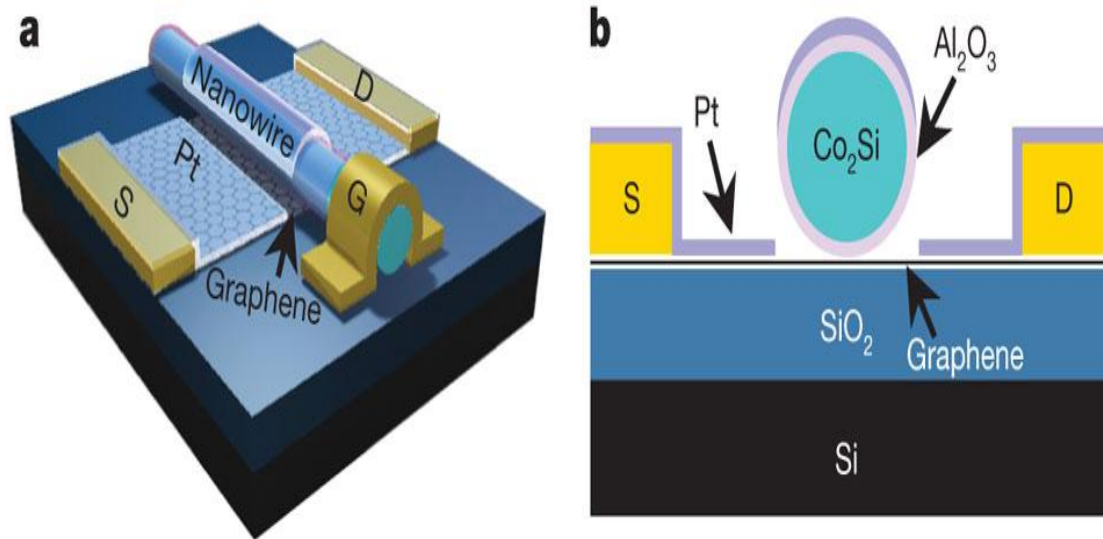


Figure 2. 4. Image of graphene based transistor [62]

2.1.1.3.3 Graphene Optoelectronics

In despite of extraordinary electrical transport properties, graphene has tremendous optical properties [52]. Exclusively, ultimate carrier mobility, transparent nature, low reflectivity and ballistic transport nature appeal for excellent agent of graphene to use in transparent electrodes. Graphene acts like a two-dimensional electron cloud, with 2.3 % absorbance of visible light are reported so far [53].

Absorption of multilayer graphene sheet is nearly proportional to the number of stacks. This absorption is linear in the range of ultraviolet (UV) to infer red (IR), very low reflectivity up to 0.1 % is reported for graphene single sheet which is promoted up to 2 % for 10 stacks of graphene layers. Hence graphene will be considered a promising candidate to use in transparent conducting electrodes (TCEs), Photo detectors, light emitting diodes (LEDs), photovoltaic (PVs) and quantum dots etc. [54-55].

2.1.1.3.4 Graphene Sensors

Graphene has drawn prominent attention for sensor applications, due to excellent adsorption for materials. The adsorption capability of graphene is due to high surface area, planer morphology, which is further improved by synthesizing graphene via wet chemical route, to induce surface defects and also by fictionalizing with different functional groups accordingly. Furthermore, the transparent nature and ultimate strength give the edge to graphene based sensor applications. In literature use of graphene in electrochemical sensors, biosensors and fluorescence sensors are successfully reported [56-57].

References

1. History of Carbon and Carbon Materials - Center for Applied Energy Research - University of Kentucky". Caer.uky.edu. Retrieved 2008-09-12
2. S. J. Tans, M. H. Devoret, H. Dai, A. Thess, R. E. Smalley, L. J. Georliga, and C. Dekker. Individual single wall carbon nanotubes as quantum wires. *Nature* 1997; 386:474–477.
3. N.H. Cho, K. M. Krishnan, D. K. Veirs, M. D. Rubin, C. B. Hopper, B. Bhushan and D. B. Bogy. Chemical structure and physical properties of diamond-like amorphous carbon films prepared by magnetron sputtering. *Journal of Materials Research*. 2011; 5: 2543-2554.
4. W Choi and J Won 2011 *Graphene: Synthesis and Applications*, 1, Lee CRC Press, Boca Raton London New York
5. J. C. Meyer, A. K. Geim, M. I. Katsnelson, K. S. Novoselov, T. J. Booth and S. Roth. The structure of suspended graphene sheets. *Nature* 2006; 446, 60-63
6. A.K. Geim. Graphene: status and prospects. *Science* 2009; 324:1530–1534.
7. A.K. Geim and K.S. Novoselov. The rise of graphene. *Nat Mater* 2007; 6:183–91.
8. Rao CNR, Sood AK, Subrahmanyam KS, Govindaraj A. Graphene: the new two-dimensional nanomaterial. *Angew Chem Int Ed* 2009; 48:7752–7777
9. Dreyer DR, Park S, Bielawski CW, Ruoff RS. The chemistry of graphene oxide. *Chem Soc Rev* 2010; 39:228–240.
10. Loh KP, Bao Q, Ang PK, Yang J. The chemistry of graphene. *J Mater Chem* 2010; 20:2277–89.
11. Boukhvalov DW, Katsnelson MI. Chemical functionalization of graphene. *J Phys: Condens Matter* 2009; 21:344205.
12. Allen MJ, Tung VC, Kaner RB. Honeycomb carbon: a review of graphene. *Chem Rev* 2009; 110:132–45.
13. X. Huang, Qi X, Boey F, Zhang H. Graphene-based composites. *Chem Soc Rev*. 2012; 10.1039.
14. C. Navarro, R. Weitz, A. Bittner, M. Scolari, A. Mews, M. Burghard and K. Kern. Electronic transport properties of individual chemically reduced graphene oxide sheet *Nano Let.* 2007; 7:3499–3503.
15. Frank, I.W Tanenbaum, D. M Zaned, A.M McEuen, and P.L McEuen *J. Vac. Sci. Technol.* 2007; 25-2558.
16. X .Du, I. Skachko, A. Barker and E. Y .Andrei *Nature Nanotechnol.* 2008; 3: 491–495.
17. J. Cai, P. Ruffieux, R. Jaafar, M. Bieri, T. Braun, S. Blankenburg, M. Muoth, A. P. Seitsonen, M.Saleh, X. Feng, K. Müllen and R. Fasel *Nature.* 2010; 466:470-473.
18. J .Yao, J. Lin, Y. Dai, G. Ruan, Z. Yan, L. Li, L. Zhong, D. Natelson and J. M. Tour . Highly transparent nonvolatile resistive memory devices from silicon oxide and graphene, *Nature Communications.* 2012; 3: 11-01.

19. C. G. Navarro , R. T. Weitz , A. M. Bittner , M. Scolari , A. Mews , M. Burghard , and K. Kern . Electronic Transport Properties of Individual Chemically Reduced Graphene Oxide Sheets. *Nano Lett*2007; 7: 3499–3503.
20. C. Schafhaeutl and J. Prakt. Chem1840; 21: 129.
21. C. Schafhaeutl .On the combination of carbon with silicon and iron, and other metals, forming the different species of cast iron, steel, and malleable iron. *Phil Mag* 1840; 16:570–590.
22. M. Inagaki. *J. Mater. Res* 1989; 4: 1560.
23. C. Hrold, A. Hrold, P. Lagrange. *J. Phys. Chem. Solids*1996; 57: 655.
24. M. Noel, R. Santhanam. *J. Power Sources*1998; 72: 53.
25. N. E. Sorokina, I. V. Nikolskaya, S. G. Ionov and V. V. Avdeev. *Russ. Chem. Bull* 2005; 54: 1749.
26. H. P. Boehm, A. Clauss, G. O. Fischer, U. Hofmann and Z. Naturf. Proceedings of the Fifth Conference on Carbon Pergamon Press, Heidelberg, Germany 1962; 73.
27. D. McNaught, A. Wilkinson, IUPAC inCompendium of Chemical Terminology (Eds. 2nd ed., Blackwell Scientific.Oxford 1997.
28. C. Berger, Z. Song, T. Li, X. Li, A. Y. Ogbazghi, R. Feng, Z. Dai, A. N. Marchenkov, E. H. Conrad, P. N. First and W. A. de Heer. *J. Phys. Chem. B* 2004; 108: 19912.
29. K. S. Novoselov, A. K. Geim, S. V. Morozov, D. Jiang, Y. Zhang, S. V. Dubonos, I. V. Grigorieva and A. A. Firsov. *Science* 2004; 306: 666.
30. S. V. Morozov, K. S. Novoselov, M. I. Katsnelson, F. Schedin, D. C. Elias, J. A. Jaszczak and A. K. Geim. *Phys. Rev. Lett* 2008; 100: 016602.
31. S. Stankovich et al. Synthesis of graphene-based nanosheets via chemical reduction of exfoliated graphite oxide. *Carbon* 2007; 45: 1558 – 1565.
32. H.C. Schnapps, J.L. Li, M.J. McAllister, H. Say, M. Herrera-Alonso and D.H. Adamson. Functionalized single grapheme sheets derived from splitting graphite oxide. *J. Phys. Chem. B* 2006; 110: 8535–8539.
33. G. Wang et al. Highly efficient and large-scale synthesis of graphene by electrolytic exfoliation *Carbon* 2009; 47:3242-3246.
34. A review of chemical vapour deposition of graphene on copper Cecilia Matte, Hokwon Kim and Manish Chowilla Received 5th July 2010, Accepted 4th October 2010 *Journal of Materials Chemistry*
35. A Burk and L.B Rowland. “The role of excess silicon and in situ etching on 4h-sic and 6h-sic epitaxial layer morphology. *Journal of Crystal Growth* 1996; 167:586–595.
36. C. Riedl et al. Epitaxial graphene on SiC (0001) to be published in *Structural and electronic properties of epitaxial graphene on SiC (0001)*. *J. Phys. D* 2010.
37. P. Blake, P. D. Brimicombe, R.R. Nair, T. J. Booth, D. Jiang, F. Schedin, L. A. Ponomarenko, S.V. Morozov, H. F. Gleeson, E. W. Hill, A. K. Geim and K. S. Novoselov. Graphene-Based Liquid Crystal Device.” *Nano Letters*2008; 8: 1704 -1708.

38. One Pot Synthesis of Graphene by Exfoliation of Graphite in ODCB Sumanta Sahoo, Goutam Hatui, Pallab Bhattacharya, Saptarshi Dhibar, Chapal Kumar 2013
39. K. moon, J. G. Rodney .s. Ruoff and H. Lee. Reduced graphene oxide by chemical graphitization. *Nature communications* 2010; 1.
40. M. Abdullah et al. J. Electrochem; Nanocomposite Graphene-Based Material for Fuel Cell Applications A. A. Elzatahry Aboubakr. *International Journal of* 2012; 7; 3115 – 3126
41. By Yanwu Zhu , Shanthi Murali , Weiwei Cai , Xuesong Li , Ji Won Suk , Jeffrey R. Potts , and R. S. Ruoff . *Graphene and Graphene Oxide: Synthesis, Properties, and Applications Adv, Mater.* 2010; 22: 3906–3924.
43. N. Liu et al. One-Step Ionic-Liquid-Assisted Electrochemical Synthesis of Ionic-Liquid-Functionalized Graphene Sheets Directly from Graphite. *Adv. Funct Mater* 2008; 18:1518-1525.
44. K.I. Bolotin , K.J. Sikes, Z. Jiang, M. Klima, G. Fudenberg, J. Hone, P. Kim And H.L. Stormer. Ultrahigh electron mobility in suspended grapheme. *Solid State Communications* 2008 ;146:351–355
45. S. Novoselov et al. Two dimensional gases of massless Dirac fermions in grapheme. *Nature*, 2005; 438: 197-200.
46. Yu, G. Liu, x. Anirudha, V. Sumant, V. Goyal, and A. A. Balandin. Graphene-on-Diamond Devices with Enhanced Current-Carrying Capacity. *Nano Letters* 2012; 1.
47. Subjecting a graphene monolayer to tension and compression Georgia Tsoukleri et al.
48. W. L. Zhi and K. Mu2llen. Transparent, Conductive Graphene Electrodes for Dye-Sensitized SolarCells 2007; Revised Manuscript Received November 1
49. Lemaitre, X. Miao, B. Gila, B.R. Appleton, and A. F. Hebard Rectification at Graphene-Semiconductor Interfaces: Zero-Gap Semiconductor BasedDiodes. *Cond-mat.mtrl-sci* 2012.
50. B. J. Kim, H. Jang, S. K. Lee, B. H. Hong, J. H. Ahn and J. H. Cho. High-Performance Flexible Graphene Field Effect Transistors with Ion Gel Gate Dielectrics. *Nano letters* 2010.
51. K. S. Novoselov, A. K. Geim, S. V. Morozov, D. Jiang, Y. Z. ng , S. V. Dubonos, I. V. Grigorieva, and A. A. Firsov. Electric Field Effect in Atomically Thin Carbon Films. *Science* 2004; 306:666–669.
52. Y. Shi, W. Fang, K. Zhang, W. Zhang and L .Jong. Small Photoelectrical Response in Single-Layer Graphene Transistors 2009.
53. F. Bonaccorso, Z. Sun, T. Hasan and A. C. Ferrari. Graphene photonics and optoelectronics. *Nature photonics* 2010.
54. Charlier, J. C. Eklund, P. C. Zhu, J. Ferrari, A. C. Electron and phonon .eir relationship with carbon properties of graphene: Th nanotubes. *Top. Appl. Phys* 2008; 111: 673–709.
55. P. Blake et al. making graphene visible. *Appl. Phys. Lett.* 2007; 91:063124.
56. Hwangl et al, Graphene as Thin Film Infrared Optoelectronic: *ACS Nano is;* 2003.

57. J. D. Fowler, M. J. Allen, V.C. Tung, Y. Yang, R. B. Kaner, and B. H. Weiller .Practical Chemical Sensors from Chemically Derived Graphene. *ACS Nano* 2009; 3: 301-306.
58. Yu Chen et al. Graphene and its derivatives, *Chem. Soc. Rev.*, 2012, **41**, 4688-4707; 2012.
59. Lei Liao, et al High-speed graphene transistors with a self-aligned nanowire gate, *Nature*: 467, 305–308; 2010.

60. Sukang Bae, Sang Jin Kim, Dolly, towards industrial applications of graphene electrodes, *Phys. Scr.* 2012; 2012.
61. Sukang Bae *et al*, towards industrial applications of graphene electrodes; 2012: *Phys. Scr.* 014024.
62. Lei Liao et al, High-speed graphene transistors with a self-aligned nanowire gate, *Nature Let.* 2010; 467:305-308.

CHAPTER 3

Introduction to Ferrites

Ferrites are the magnetic mix metal oxides comprising the ferric ions as an essential constituent, while in mineralogy or in metallurgy the term ferrites refer to that material having a cubic crystal structure of spinal mineral. The ferrites application has been known from ancient times for multiple centuries. Magnetite or ferrous ferrite is a naturally occurring ferrite, the Chinese found its use in the loadstone (i.e. Fe_3O_4) due to its weak permanent magnetism for navigation purposes as early in the 12th century [1-2].

Hilbert a German scientist, in 1909 reported first systematic study on the relation between magnetic and chemical properties of many iron oxides, but faced hurdles to identify its magnetic phases. However near to 1930s modern ferrites were investigated by Forestier, Hilppert and Wille for their structural, magnetic and electrical properties. Japanese scientist's attempted to study magnetic oxides from 1930s to 1935, Snoek and co-workers were studying the ferrites in 1936; they found that one of the important properties of ferrites to use as core for inductors is the loss tangent per permeability, so called loss-factor [3].



Figure 3.1: Ferrites devices in different shapes [1]

They also investigated that loss can always be minimized by introducing an air gap and the permeability not effected adequately. This finding, led Snoke to develop manganese-zinc ferrite, of low loss and ultimate permeability. It was 1945, that Snoke coined the physical and technological applications of modern ferrites and a

new field of science came into being. Since that time ferrites brought stormy revolution in electrical and electronic areas, to improve its capability and endurance [4-6].

3.1 Structure of Ferrites

Ferrites crystallize in three types of structures.

- ✚ Garnet Ferrites: These are also cubic structural ferrites but with general formula $\text{Ln}_3^{3+}\text{Fe}_5\text{O}_{12}$, here Ln maybe, EU, Tb, Tm, Ho, Er, Gd or Ln [7].
- ✚ Magnetoplumbite ferrites: With hexagonal structure, having general formula $\text{M}^{2+}\text{Fe}_{12}\text{O}_{19}$, where M may be Sr or Ba [8].
- ✚ Spinal ferrites: Having cubic crystalline structure with general formula $\text{M}^{2+}\text{Fe}_2\text{O}_4$, here M may be any metal such as Mn, Cd, Fe, Co, Cu, Mg or Al [9].

Spinal ferrites are the most simplest structure, crystallizes among the three ferrites groups.

The spinal ferrites unit cell is comprised mainly of oxygen lattice, having 32 oxygens, 16 trivalent irons along with 8 divalent metal ions, as shown in figure. 5 .

An interesting feature of oxygen lattice is its ions are arranged in face centered cubic structure, such that two types of interstitial sites are produced, at A site tetrahedral co-ordinate and octahedral B sites. The whole unit cell consists of two groups of four cubes. The positions of the ions are changing in these groups may share corners, faces or edges.

Each group having four oxygens (Large spheres), located diagonally on each accountant and also on the tetrahedral corner. The tetrahedral oxygen ions surrounding the metal ions located in the center of the left hand side octant (small sphere, not shaded). This ion appeal to occupy A site of the intrinsic position produced by oxygen.

The second ionic group on right hand contains four metal ions enclosed by an octahedron resulted from six oxygen ions, and goes to fill the B site. Hence each unit cell consists of 64 A sites, only 8 of which are occupied and remaining unoccupied free sites. B sites are 32 in number, 16 of which are occupied [4-5].

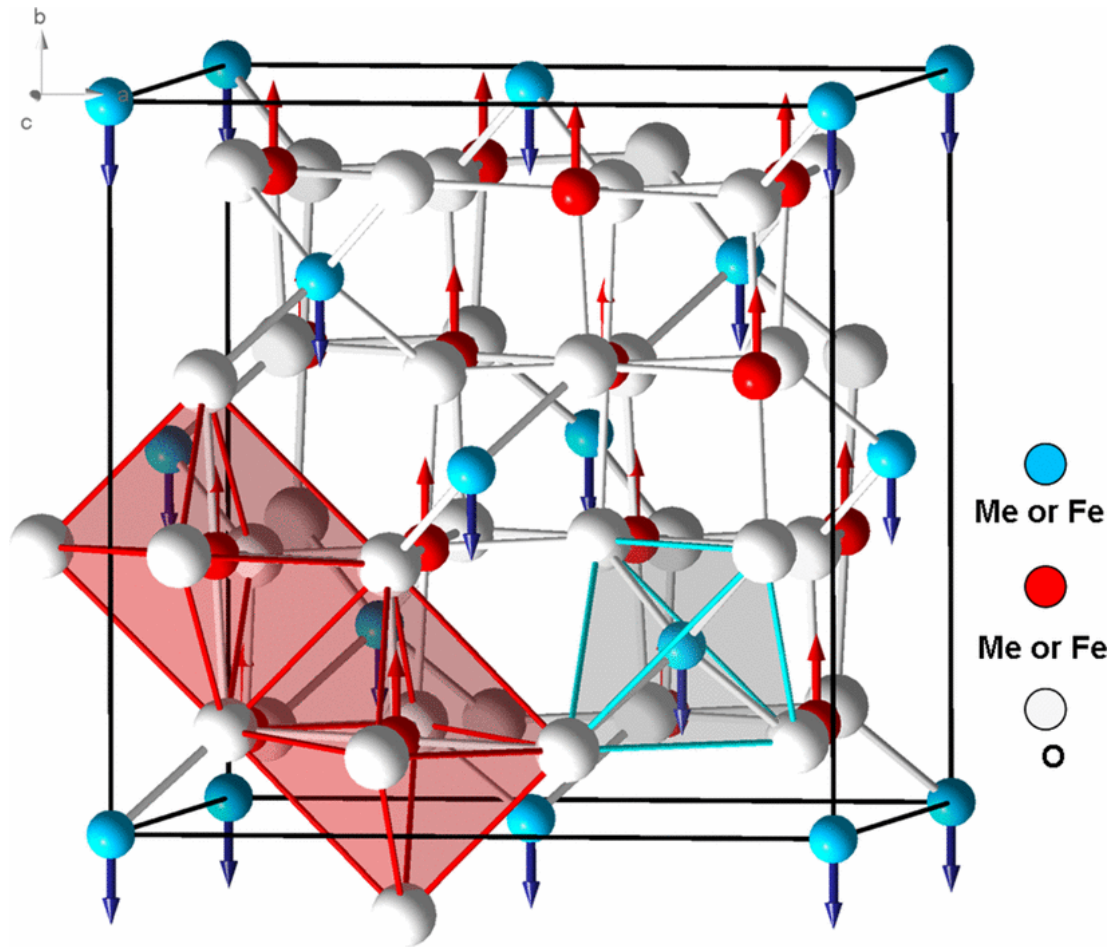


Figure 3.2 Structure of ferrite [16]

3.2 Synthesis Routes of Ferrites

As we are interested in ferrites composites, so we have to evaluate nano ferrites synthesis techniques, while coarse ferrites are produced by traditional ceramic processing. Nano particles ferrites are superior due to large surface area, very small size, high surface energy and excellent properties [9-10].

Bottom –up and top-down approaches are reported so far, in bottom-up we take molecules or atoms to manipulate these in a systematic way to get the desired shape, size and properties of specific ferrite materials. In top-down approaches the bulk materials are broken down repeatedly until we get nano sized materials. Mechanical attrition done in high energy ball milling is an example of top-down approach.

Synthesis routes may be generally classified in two ways, the physical way (involving only physical changes such as phase, shape and size of the matter) and chemical way (where permanent or chemical change occurs). Bottom-up techniques as lithography, ball milling and screen printing are all physical synthesis routes. Some chemical routes for nano ferrites synthesis are sol-gel, hydrothermal and co-precipitation reported from various laboratories [11-12].

3.3 Properties and Applications

Ferrites are used in almost every electrical and electronic devices, it finds its use in the applications from simple lifting magnets to complex electrical and communication systems. Demand for ferrites is increasing rapidly due to the advancement in modern technology, such as satellite communications, radar systems, memory and advance computer applications. The major upsurge for the passion of ferrites research is due to the development of modern small and fast power supplies, which are being used in cell phones, computers, communications, microprocessors and entertainment applications [13].

Ferrites coined its modern use, first in a powerful application to enable the time dependent magnetic deflection of the electron array, in a television receiver. Mn-Zn ferrite emerged as an excellent candidate for core material in line-time-base and e.h.t transformer. Another excellent area of use was the field-shaping the yoke for beam deflection system in the picture tube. Latter on, several ferrites compositions i.e Mg-Zn, Ni-Zn and Li-Zn etc. were applied for yokes application due to higher resistivity to enable direct winding of the coils on ferrite. However high efficient TV deflection yokes are fabricated from Mn_Zn ferrite. Also ferrite rods and plates make it possible to make the compact antennas for radio receivers [12-14].



Figure 3.3. Digital TV receiver contains Mn-ferrites deflection yokes [17]

The need for use of ferrites in line communication systems started, when the analog frequency divisions multiplex (FDM) systems demand for large numbers of ultimate performance, transformers and inductors operating in the frequency range from 40 kHz to 500 kHz. Ferrites were selected an excellent agent for core materials in these applications, due to a combination of high resistivity along with good magnetic nature. Their large frequency range along with ultimate resistivity successfully replaced the conventional metallic magnetic materials and further enabled FDMs to operate over wide and higher frequency range [15].

Other important applications of ferrites are summarized below.

- Flyback transformers [16]
- Fitter inductors [17]
- Magnetic amplifier [18]
- Antenna cores
- IF transformers
- Magnetic switches and memories
- Magnetic drug delivery systems.

References

1. V. Pallai and D.O Shah, Journal of Magnetism and Magnetic Materials 163, 243-248, (1996)
2. R Skomski, J. Phys.: Condens. Matter 15, R1-R56, (2003).
3. High Magnetostrictive Cobalt Ferrite for Sensor Application O. F. Caltun ,G.S.N.Rao ,K.H.Rao , B. Parvatheeswara Rao CheolGi Kim, Chong-Oh Kim, I. Dumitru , N. Lupu , and H. Chiriac sensor letters Vol.5, 1–3, 2007
4. July 1999 Materials Letters 40 1999 39–45www.elsevier.com locate matlet
5. G. Ranga Mohan a, D. Ravinder a , A.V. Ramana Reddy a , B.S. Boyanov ,Dielectric properties of polycrystalline mixed nickel–zinc ferrites 1999.
6. I. Subramanian, m.n. Afsar, k.a. Korolev , Com 179 -20 millimeter wave material characterization of strontium ferrites using magneto-optical approach .
7. A.S. Logginov, G.A. Meshkov, V.A. Nikolaev, A.P. Pyatakov , Magneto electric Control of Domain Walls in a Ferrite Garnet Film Physics Department, M.V. Lomonosov MSU, Moscow, Russia, 119992;
8. W. Eerenstein, N. D. Mathur & J. F. Scott, Multiferroic and magnetoelectric materials, Nature, 442,759 (2006).
9. Özgür et al., Microwave Ferrites, submitted to Journal of Materials Science: Materials in Electronics, 2009.
10. E. Manova, D. Paneva, B. Kunev, Cl. Estournès, E. Rivière, K. Tenchev, A. Léaustic, I. Mitov. Mechanochemical synthesis and characterization of nanodimensional iron-cobalt spinel oxides. Journal of Alloys and Compounds, 485 (1-2): 356-361, 2009
11. Z. Zi, Y. Sun, X. Zhu, Z. Yang, J. Dai, W. Song. Synthesis and magnetic properties of CoFe O ferrite nanoparticles. Journal of Magnetism and Magnetic Materials, 321 (9): 1251-1255, 2009.
12. H. Gul, A.Maqsood. Structural, magnetic and electrical properties of cobalt ferrites prepared by the sol-gel route. Journal of Alloys and Compounds, 465 (1-2): 227-231, 2008.
13. Q. Liu, J. Sun, H. Long, X. Sun, X. Zhong, Z. Xu. Hydrothermal synthesis of CoFe Onanoplatelets and nanoparticles. Materials Chemistry and Physics, 108 (2-3): 269-273, 2008.
14. I.Sharifi, H. Shokrollahi, M. M. Doroodmand, R. Safi, Magnetic and structural studies on CoFe₂O₄ nanoparticles synthesized by co-precipitation, normal micelles and reverse micelles methods, Journal of Magnetism and Magnetic Materials, 324 (10): 1854-1861,
15. M Saidani a and MAM Gijs , applied physics letters volume number may 2004 High-quality radio-frequency inductor son silicon using a hybrid ferrite ,November 2003; 2004.
16. W. Eerenstein, N. D. Mathur & J. F. Scott, Multiferroic and magnetoelectric materials, Nature, 442,759 (2006).
17. <http://obsolete.tellyemuseum.blogspot.com/2011/10/wega-color-3016-chassis-internal-view.html>.

18. Alain Tran, Miodrag Bolic, and Mustapha C.E. Yagoub , Magnetic-Field coupling characteristics of ferrite-coil antennas for low-frequency RFID applications; IJCSI International Journal of Computer Scienc.7:2010.

CHAPTER 4

Microwave Shielding, Problems and Solutions

Electromagnetic waves, in the wavelength range from millimeter to one meter, refer to microwave. Lying in the wave spectrum, from 300 MHz to 300 GHz, frequency range [1].

Generally, the minimum limit of microwave is considered to include the full ultimate frequency range from 3 to 30 GHz, while in RF (radio frequency) science often limiting the lower range at 1 GHz frequency, and upper frequency ranges up to 100 GHz [2].

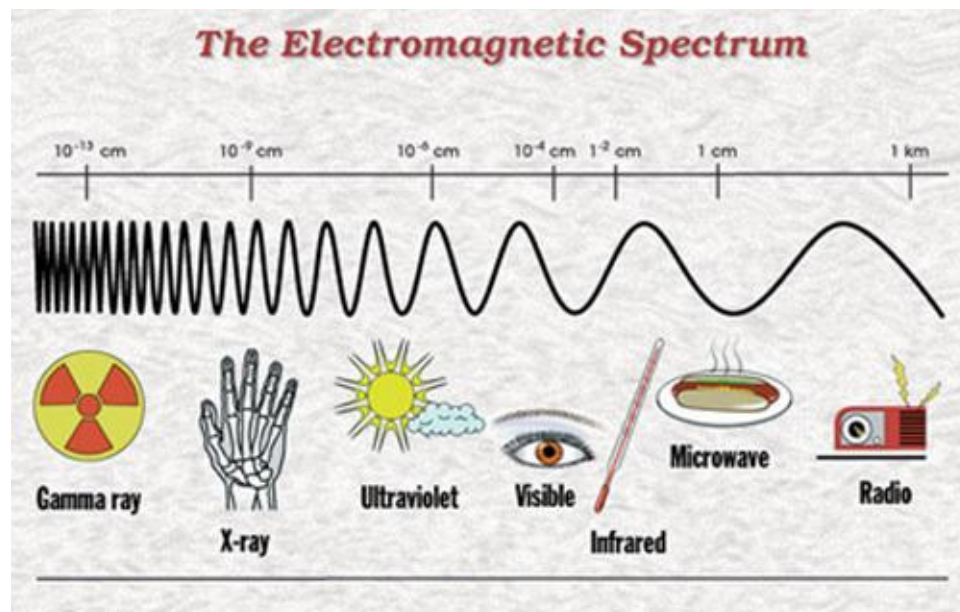


Figure 4.1 the range of microwave spectrum [14]

4.1 Use of Microwave

In early 1950s most of the long-distance telephone communications were carried through microwave networks, before the emerging of fiber optic technology. More than 5000 telephonic relays were combined on single microwave channel and send via frequency-division-multiplex (FDM). Several microwave channels could be combined into a single transmitting antenna for caper to the next station, more than 60 km away [3].

MB-Wireless Access (MBWA) used microwaves in frequency ranges from 1.6 GHz to 2.3 GHz; provide excellent mobility and in-structure transmission like mobile phones, more efficiently. GSM communication of mobile phone networking, use high UHF or low microwave frequencies from 1.9 GHz to 1.8 GHz, while U.S is using 2.3 GHz frequency for satellite radio. Microwave is used in telecommunication and broadcasting transmissions due to spectrum comprising larger bandwidth

compare to radio spectrum, shorter wavelength, and needed smaller directional antennas [4].

Most of the satellite communications systems are operating in the microwave bands of K_u , K_a , X and C, these ranges of frequency make possible the safe operation of satellite communications by preventing congested UHF band and also avoid EHF absorption by the atmosphere. TV via satellite uses K_u band for direct broadcasting service, while C band for ordinary fixed satellite communications. Another interesting use of microwaves is for cooking applications in microwave ovens, as it vibrates the molecules of water and foodstuffs hence are heated rapidly [5].

Some major areas of microwave applications are summarized below

- Telecommunications
- Radar
- Traffic speed camera
- Radio astronomy
- Spectroscopy
- Medical treatment
- Navigation and military applications

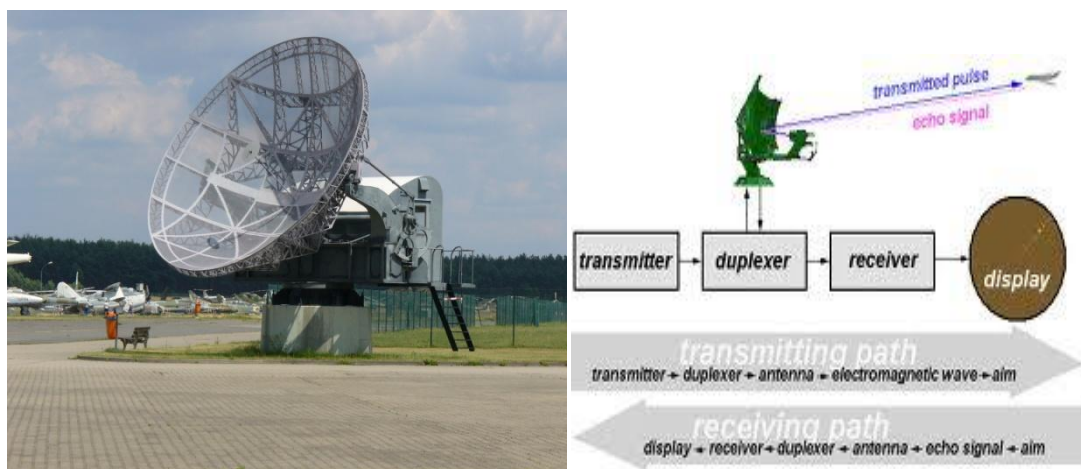


Figure 4.2 Radar and its function [15]

4.2 Issues Caused By Microwave

Microwave have two types of adverse effects, one directly on living organisms (biological issue) and second on the operations of electrical instrumentations due to induction with other electromagnetic radiations.

4.2.1 Biological Issue

This issue is not so conflicting, as no such evidence exists that any disease caused purely due to normal microwave dosing. The reason behind is that the microwave does not contain enough energy to ionize any substance chemically, and a type of

non-ionizing radiation. However according to some reports, long term microwave exposure may cause cancer in some tissues. Apart from cancer microwave may cause burning due to vibrating protein and water molecules within the human body. Another issue was experienced caused by microwave, the people responsible for radar operation felt some auditory problems, identified as the cause of microwave induction in the hearing site within the brain [6].

Some reports address that microwave cause's cataract in the human eye by denaturing proteins of the eye-lens. The cornea and eye-lens is the most susceptible organs due to absence of bloods, which is responsible for heat conduction, hence the heat caused by microwave accumulate and affect the eye-lens [7].



Figure 4.3 Cataract in the human eye caused by microwave [7]

4.2.2 Electromagnetic Noises

Electromagnetic interruptions produced due to voltage and alternating current which results the induced signals (current and voltage), in the electronic circuits, present in its premises. These noises tend to deface the performance of electronic systems. Electromagnetic disturbances within communication pathways, process control and automation may result loss of energy, time, resources and some time human health also [8]. In petroleum services, robotic based operation theatres and during flight, use of mobile phone is forbidden to avoid spoilage of electronic failure or other serious scenario.

The warship of the 20th century is decorated with a huge electronic system, comprising of countermeasure systems, target-acquisition and navigation radar, and a lot of communication machinery mounted on the single metal structure. This compact electronic system may cause two major problems, system to system communication hindrance and false imaging due to self reflections. For effective military operation, such problems should be avoided otherwise severe condition may face.

4.3 Microwave Shielding

A lot of efforts have been done so far, to prevent the above problems regarding microwave and various types of solutions are addressed. Base of Microwave shielding is either to absorb or reflect back these electromagnetic waves, to restrict its emitting, outside of the core channel. However the best solution is that, to shield the electromagnetic device without affecting its operation [9-10].

4.3.1 Dielectric Material Absorber

Ferrites are metal oxides having dipoles in their lattice structure and hence experience enough polarization. Its complex permeability is far different than its complex dielectric constant and hence cause interface reflection to absorb the coming RF wave.

4.3.2 Resonant Absorbers

Resonant absorbers are the simplest technique for RF shielding, Consists of Salisbury screen spaced $\frac{1}{4}$ of wavelength from a ground conductive plane. The resonant sheet need to be thin as possible having resistance up to $300 \Omega/m^2$ compared to free space [11].

Refer to Figure 4.4, an incident wave partially passed and partially reflected back transmitted part of the incident wave undergoes several mutual reflections and series of emergent waves are produced. The resonator frequency is designed in such a way that net emergent wave and reflected part, both equal in amplitude but out of phase with each other. Hence theoretically zero reflection is achieved, while practically more than 30 dB absorption may be acquired.

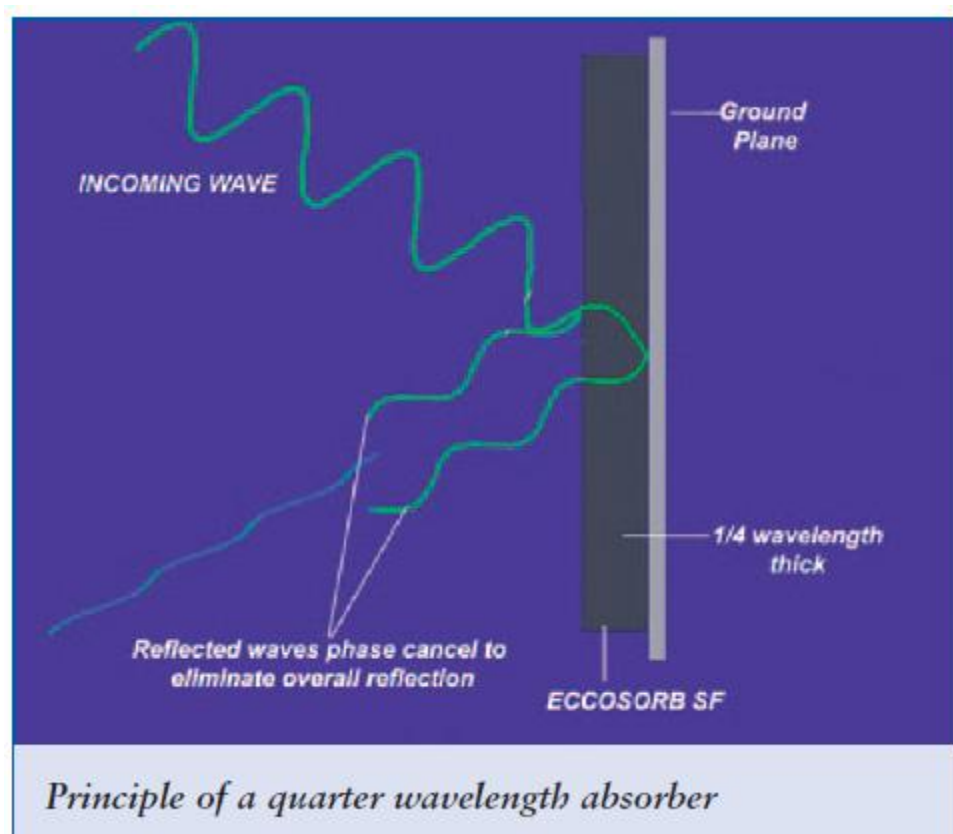


Figure 4.4 Principle of a quarter wavelength absorber [15]

4.3.3 Graded Dielectric Absorbers

This type of absorber is operating on the principle of impedance compression. In detail, the pyramidal shaped structure try to taper the impedance gradually from the free space to a condensed (loosy) area. If the structure is designed accurate and precisely then this phenomena occurs smoothly to demolish the RF interference, with a small reflection from the plane surface.

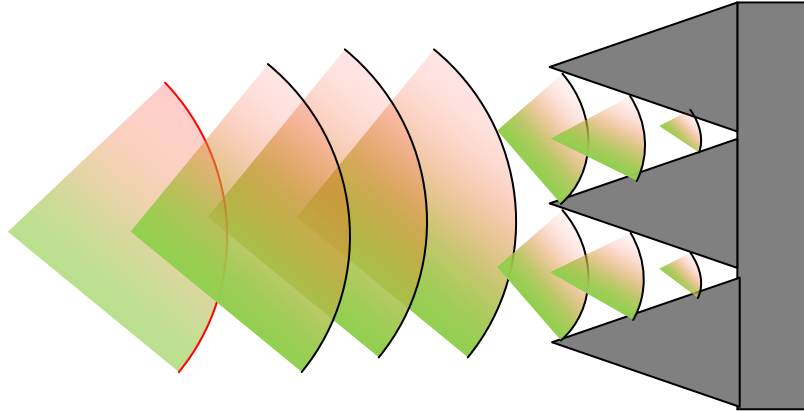


Figure 4.5, Schematics of graded dielectric absorber

The absorbing media in such types of absorbers are mainly carbon base hybrid structures, with thickness up to 30 mm. Due to the large thickness require in graded dielectric (GD) type absorbers, it is not suitable to use for radar cross section (RCS) reduction and EMI applications [12-13].

References

1. J.P. Gupta, ci JI Vol 38, No.3, July 1988, Radiation Hazards from Radars and other HighPower Microwave Generators Pollution Monitoring Section Bhabha Atomic Research Centre, Bombay; pp 287-292.
2. klaudiusz grübel, and alicja. Machnicka Impact of microwave disintegration on activated sludge, ecological chemistry and engineering, vol. 18, no. 1, 2011.
3. Politecnico di Torino Mohamed Sayed .Modern RF and Microwave Measurement Techniques Part of The Cambridge RF and Microwave Engineering Series Valeria Teppati, ETH Zürich, Switzerland Andrea Ferrero, , Microwave and Millimeter Wave Solutions, Santa Rosa View all contributors Published: July 2013 format: Hardback isbn: 9781107036413.
4. Schmitt, Ron (2002). *Electromagnetics Explained: a handbook for wireless/RF, EMC, and high-speed electronics*. Burlington, MA, USA: Elsevier. p. 343. ISBN 978-0-7506-7403-4. Retrieved 3 December 2012.
5. Method and apparatus for heating dielectric materials (21-Feb-1939)
Application Number: US 158553 A Filing Date: 11-Aug-1937
6. Labuza and T. Meister. An Alternate Method for Measuring the Heating Potential of Microwave Susceptor Films" *J. International Microwave Power and Electromagnetic Energy* 2011; 27: 205–208.
7. F. Watanabe, K. Abe, T. Fujita, M. Goto, M. Hiemori and Y. Nakano. Effects of Microwave Heating on the Loss of Vitamin B (12) in Foods". *J. Agric. Food Chem* 1021; 46: 206–210.
8. s. k. singh , r. menon, d. senthil kumar, r .venkateswaran, m. r .kulkarni, p .c. saroj,k. v. nagesh, k. c. mittal and d.p.chakravarthy. Measurement of high-power microwave pulse under intense electromagnetic noise. *Journal of January Physics* 2010; 74: 123-133.
9. m. y. koledintseva, j. drewniak and r. dubroæ. Progress in electromagnetic research b, modeling of shielding composite materials and structures for microwave frequencies, vol. 15, 197 {215, 200
10. Fox, R. T., V. Wani, K. E. Howard, A. Bogle and L. Kempel. Conductive polymer composite materials and their utility in electromagnetic shielding applications. *Journal of Applied Polymer Science* 2008; 107:2558-2566.
11. toscano, k. b. alici, e. ozbay and l. ve gni. IEEE Transactions on Electromagnetic Compatibility, vol. 53, no. 1, february 2011 63 design of miniaturized narrowband absorbers based on resonant-magnetic inclusions filiberto bilotti , senior member.

- 12.
13. S. M. Abbas, r. P. R. C. Aiyar and o.m. Prakash .Synthesis and microwave absorption studies of ferrite paint. Bulletin of materials science 1998; 21 :279-282.
14. Devender and S.R. Ramasamy A review of EMI shielding and suppression materials Res. Center Imarat, Hyderabad 01/1998; DOI:10.1109/ICEMIC.1997.669850 ISBN: 81-900652-0-3 In proceeding of: Electromagnetic Interference and Compatibility '97. Proceedings of the International Conference.
15. <http://mail.colonial.net/~hkaiter/electromagspectrum.html>
15. 15 Qi-Ye Wen et al. Perfect Metamaterial Absorbers in Microwave and Terahertz Bands, State Key Laboratory of Electronic Films and Integrated Devices, University of Electronic Science and Technology of China.

Chapter 5

Materials and Methods

5.1 Materials

Sulphuric acid (H_2SO_4) (98%), hydrochloric acid (HCl), acetic acid (100%) all analytical grades and Graphite Flakes (20 μm) were provided by Sigma Aldrich. Nitric acid (HNO_3) was purchased from Fisher Scientific and potassium permanganate (KMnO_4) from Sharlau Chemicals. All the chemicals were used as received.

Sodium nitrate (NaNO_3)

Hydrazine hydrate (H_2O_4)

Ammonia (NH_3)

Sodium borohydride (NaBH_4)

Iron salt ($\text{Fe}(\text{NO}_3)_3 \cdot 9\text{H}_2\text{O}$)

Cobalt salt ($\text{CoCl}_2 \cdot 6\text{H}_2\text{O}$)

5.1.2 Equipment Used

Magnetic stirring hot plate

Centrifuge


Vacuum oven

Heating furnace

Sonicator

5.2 Characterization Techniques

Various characterizations needed, to check the successful formation of target materials. During the synthesis phase I used various techniques to characterize graphene, graphene oxide and graphene based composites, some of which are quantitative like EDX, FTIR and mechanical testing and other qualitative such as surface morphology, topography and crystallinity etc. Following are the major characterization tools used.

 XRD

- ✚ FTIR
- ✚ Raman Spectroscopy
- ✚ SEM and EDX
- ✚ AFM (atomic force microscopy)
- ✚ Electrical characterization
- ✚ Mechanical characterization

5.2.1 XRD

This is the basic technique which reveals information about the bulk composition, crystal structure, and dimensions of a unit cell of the crystal, phase identification and product purity. XRD works on the principle of three dimensions diffraction grating of X-Rays. In detail, monochromatic beam of X-Rays is produced by a cathode-tube, which is focused on the sample. Intensity is recorded by a rotating detector as the rotating sample reflects the incident beam of X-rays. According to Bragg's law [1],

$$2d\sin\theta = n\lambda$$

Here d is a lattice spacing, θ is the angle and λ is the wavelength of incident X-rays

If the geometry of materials matches with that of an incident X-rays beam, interference occurs constructively and high intensity characteristic peak is recorded [2-3]

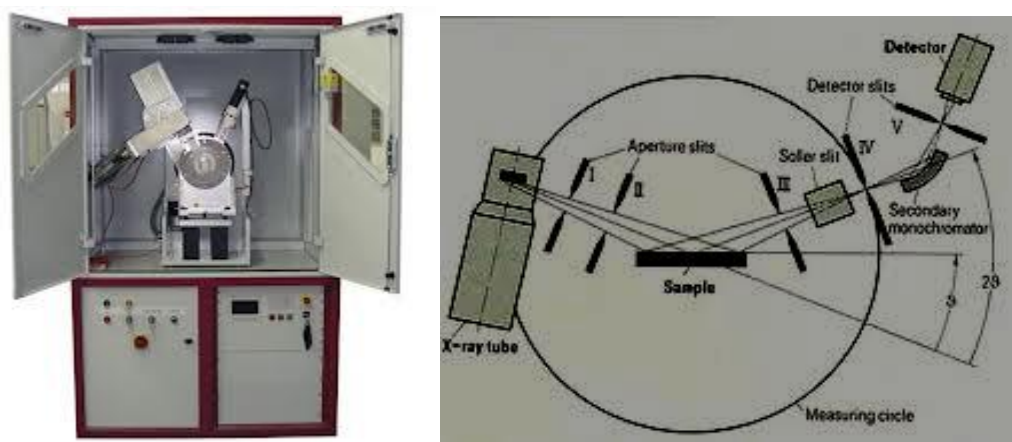


Figure 5.1 XRD unit and its working schematics [14]

Important features of XRD peak are intensity, peak position relative to 2-theta and peak sharpness. X-rays diffraction analysis of synthesized samples was carried out by XRD machine (STOE theta-theta), to confirm its structures and phase formation.

5.2.2 FTIR Spectroscopy

It is the characterization tool to explore the present bonding of a material [4]. It works on the principles of resonance produced due to the matching of the frequency of the incident electromagnetic wave (in infrared region) to that of the vibration of different bonds and functional group presents [5-6].

Fourier transform spectroscopy was performed on samples with KBr pellets by Perkin Elmer 100 series in the range from 400 cm^{-1} to 4000 cm^{-1} .

5.2.3 Raman Spectroscopy

Raman is a nondestructive technique used for material characterization. Raman spectroscopy deals with the vibration of crystal lattices and molecular bonding, as to reveal information about bonding, composition, phase and most importantly the crystal structure in all three physical states of matter. Monochromatic beam of photon directed to the sample, some of it absorbed and reflected while a little portion of it interacts the inner material. The incident photon gives its energy to the electrons to excite, on coming back to ground state emit the characteristic photons which are detected and plotted in the form of a spectrum. Raman analysis was performed by Lab RAM 800HR, made HORIBA, in the range of 1100 cm^{-1} to 2800 cm^{-1} on graphene oxide samples to study its exfoliation [7-8].

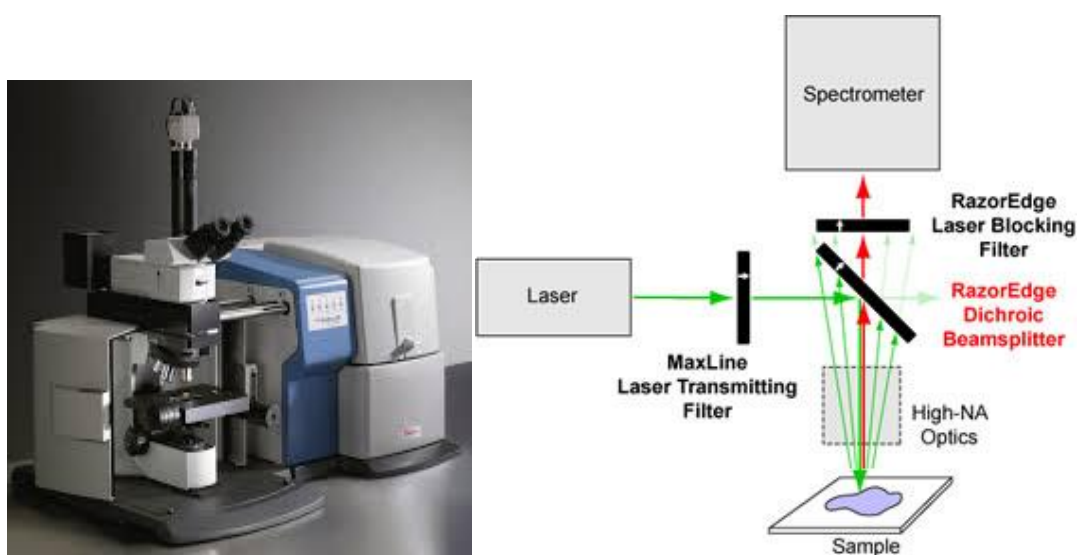


Figure 5.2 Raman spectroscope and its working diagram

5.2.4 SEM Analysis

To see the morphology, shape and particle size of material on high magnification, the scanning electron microscope is used. Similar to optical microscopy this technique use a beam of electrons instead of light to scan over the samples. These electrons go to interact with material and emit the characteristic electrons like back scattered , secondary and elastically scattered electrons along with characteristic X-rays, All these signals are detected separately through ultimate sensitive detectors. The processing system attached to SEM gathers all this information to create a 2D image of the analyzing sample [9].

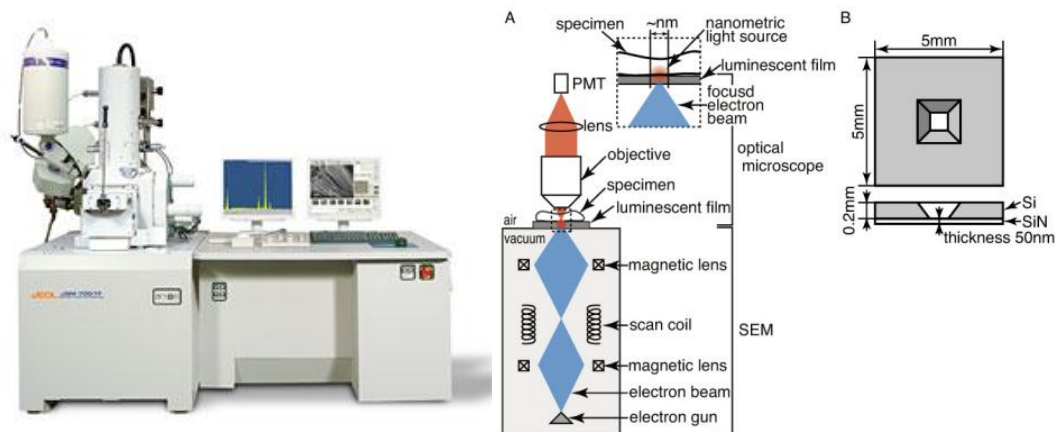


Figure 5.3 Analytical scanning electron microscope

Morphology and shape of GO, RGO flakes and composite samples were studied by Scanning Electron Microscope (JSM_6490A). The further chemical composition of all the samples was confirmed by energy dispersive spectroscopy (EDX). It uses characteristic X-rays to reveal the information about the chemical composition of the material [10-11].

5.2.5 AFM

Atomic force microscopy is a topographical technique used to evaluate the surface topography and 3D images of particles. It consists of a cantilever having an atomic scale tip on its end, the tip scans the whole surface and creates the 3D topography of the surface. There is an equilibrium distance remaining between the tip and the surface, such that atomic forces like van der Waals and short range repulsive forces balance each other. The tip moves according to the surface topography up and down, laser falling on the cantilever is reflected and sensed by the diode directed toward the coming laser light [12-13].

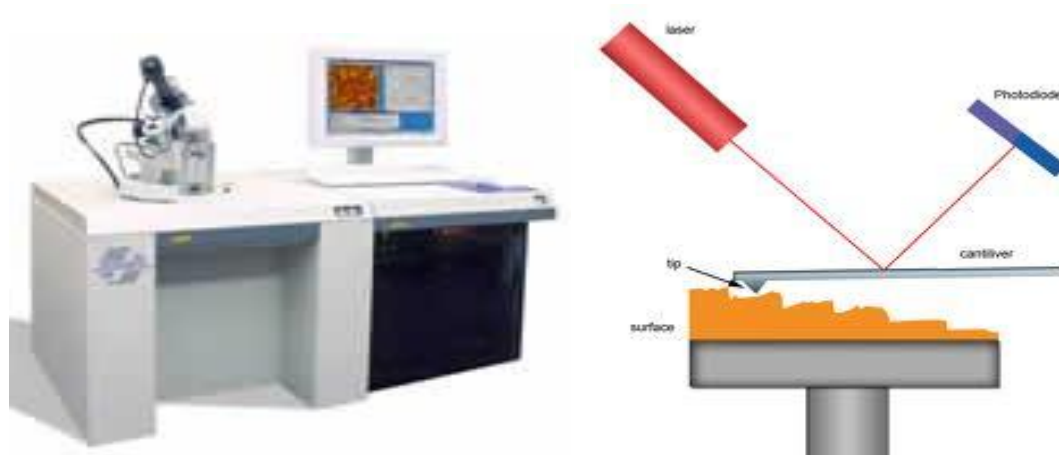


Figure 5.4 Scanning probe microscope with AFM demonstration

To measure the GO flake thickness we prepare the samples on silica substrate and 0

5.2.6 Electrical Measurements

Both the permeability and permittivity of our samples were measured by Agilent RF Impedance-Material analyzer (model#E4991A) [15], over the entire range from 1 MHz to 3GHz, with using 16453A test fixture for permittivity and 16454A for permeability on normal and torrid samples respectively.



Figure 5.5 Agilent RF Impedance-Material analyzer (model#E4991A), and its different fixtures.

The instrument using capacitance method for permittivity measurements, while the slanted relation was used for calculating the dielectric constant (ϵ_r) [16].

$$\epsilon_r = \frac{Cd}{\epsilon_0 A} \quad (1)$$

Here C is the measured capacitance in farad, d is the height in meters, ϵ_0 is the permittivity constant of free space and A is the cross-sectional area of the sample pellets.

The relative permeability for torrid samples was calculated from the measured permeability parameters by using the following standard formulae [15].

$$\mu_r = \frac{2\mu(L - L_s)}{\mu_0 h \ln\left(\frac{c}{b}\right)} + 1$$

(2)

Where L is the inductance of the torrid sample, L_s is the inductance of empty 16454A test fixture, and μ_0 is the permeability of free space while h, c and b are the thickness, outer and internal diameter of the torrid sample. L_s is further calculated with the help of the following relation [15],

$$L_s = \frac{\mu^e}{2\pi} h_0 \ln \frac{e}{a} \quad (3)$$

Where h_0 , e and a is thickness, internal and outer diameters of fixture with out the sample.

Finally the reflection loss was calculated by the following relations

$$Z_{in} = \left[\frac{\mu r}{\epsilon r} \right]^{\frac{1}{2}} \tanh \sqrt{[(j(2\pi f d/c)(\mu r * \epsilon r)]} \quad (4)$$

$$R(dB) = 20 \log_{10} \left[\frac{Z_{in} - 1}{Z_{in} + 1} \right] \quad (5)$$

Where c is the velocity of light and μr , ϵr are the relative permeability and permittivity respectively.

5.2.6.2 Die design

For permeability measurements torrid samples are needed so we have designed a die according to Agilent fixture (16454A), shown in Figure 16 and then fabricated it in the workshop of PAF base karma from die steel.

5.2.7 Mechanical characterizations

5.2.7.1 Flexural Strength

To evaluate the strength of our RGO and cobalt ferrites samples we performed the flexural test on the sintered pellets according to ASTM standard (F394-78) [17]. It is actually a ring-on-ring of disk shape samples for ceramics. Finally biaxial flexural strength was calculated using the relation [18].

$$S = 0.2387F(R - r)/d^2 \quad (6)$$

Here F is the maximum load applied before fracture and r are the outer ring diameter and inner ring diameter, while d is the height of testing pellet under load.

5.2.7.2 Micro Vickers Hardness

To measure the hardness of our samples we used Vickers diamond indenter techniques according to ASTM standard (C 1327 – 03) [19].

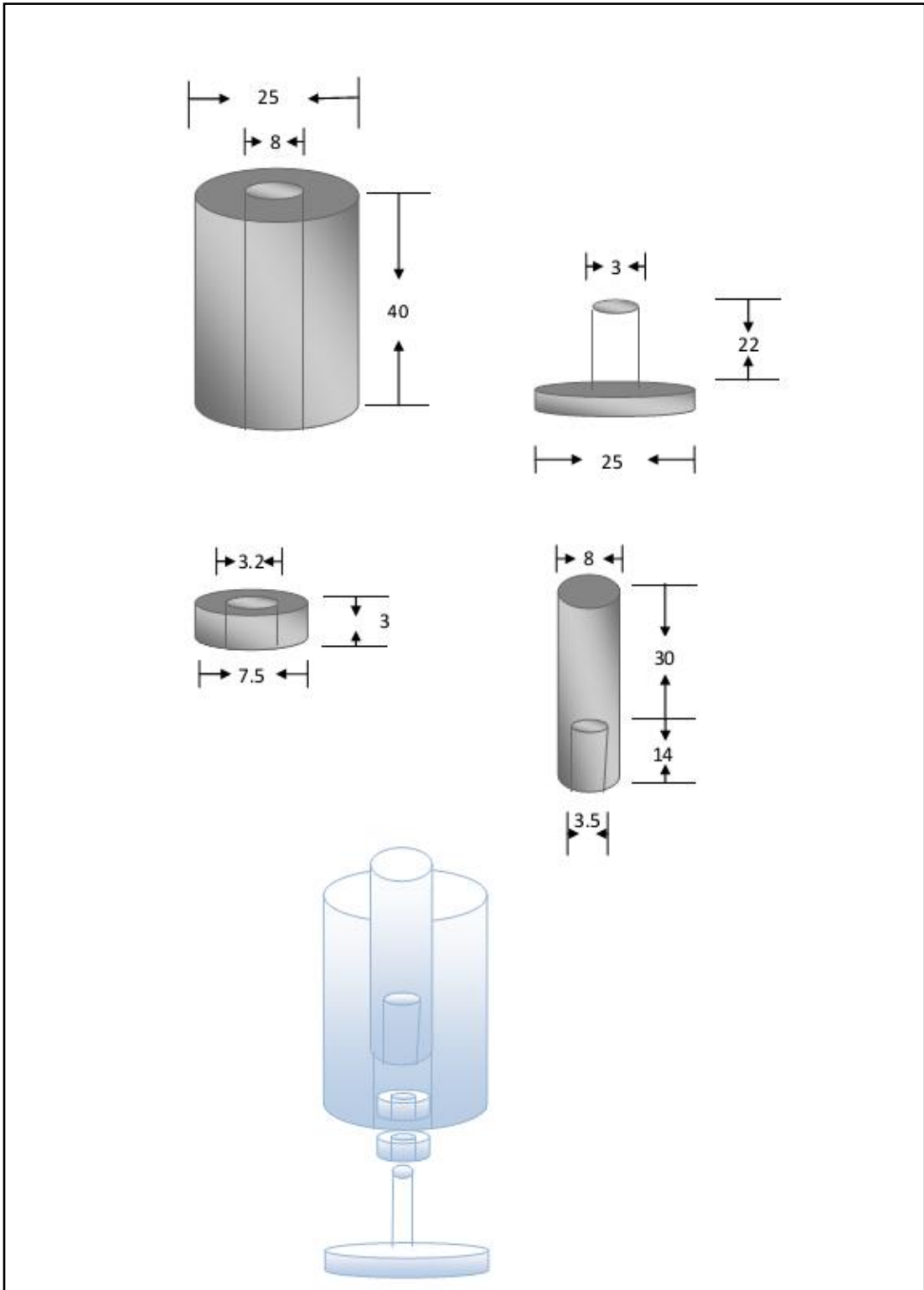


Figure 5.6 Design of die for torrid samples, all measurements are in mm.

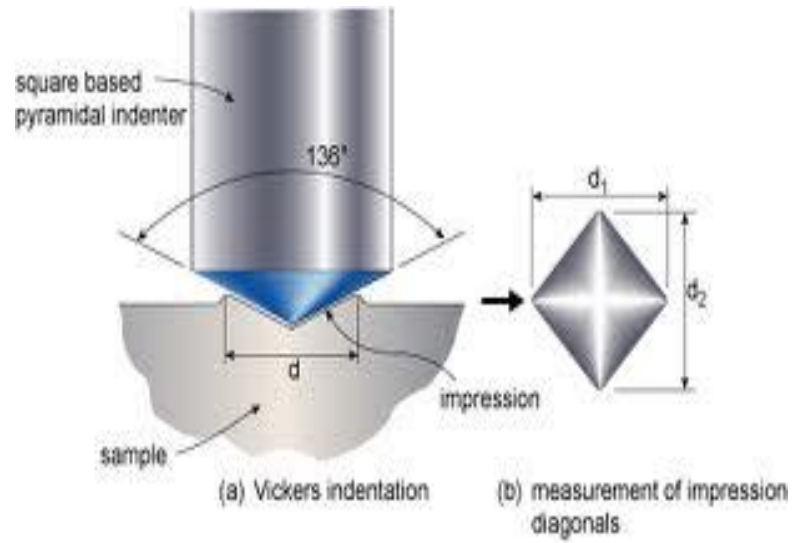


Figure 5.7 Schematics of Vickers hardness test indents [18]

For reliable results the diagonal measurements were performed by JEOL SEM. Vickers Hardness no (Hv) were calculated by the formula [20],

$$HV=1.8544 (P/d^2)$$

Where

P = load in kgf, and

D = average length of the two diagonals of the indentation in mm.

For getting true value of hardness by statistical approach we took five readings for each sample and then found its mean which was considered as true value of hardness.

References

1. W. L. Bragg and P. R. Soc. The structure of some crystals as indicated by their diffraction of X-rays. *Elements of X-ray Diffraction* 1913; 89: 248.
2. And Ed by B. D. Cullity Addison Wesley 1978.
3. B.E. Warren, General Publishing Company. *X-ray Diffraction* by 1969: 1990.
4. Griffiths, P. d. Hasseth, J.A. (18 May 2007). *Fourier Transform Infrared Spectrometry* (2nd ed.). Wiley-Blackwell. ISBN 0-471-19404-2.
5. Chamberain, J. Gibbs and J.E. Gebbie. The determination of refractive index spectra by fourier spectrometry. *Infrared Physics* 9: 189–209.
6. W. H. Smith and U.S. Patent. Digital Array Scanned Interferometer, issued Dec. 11, 1990 4,976,542.
7. R.K. Khanna. Raman-spectroscopy of oligomeric SiO species isolated in solid methane. *Journal of Chemical Physics* 1981; 74 : 2108.
8. R. S .Chao, R.K. Khanna and E.R. Lippincott . Theoretical and experimental resonance Raman intensities for the manganate ion. *J Raman Spectroscopy* 1975; 3 : 121.
9. D.McMullan. Scanning electron microscopy. " *Scanning* 2006; 17: 1928–1965.
10. Goldstein, G. I. Newbury, D. E. Echlin, P. Joy, D. C. Fiori and C. Lifshin, (1981). *Scanning electron microscopy and x-ray microanalysis*.
11. G. D.Danilatos. (). Theory of the Gaseous Detector Device in the ESEM. *Advances in Electronics and Electron Physics*. Advances in Electronics and Electron Physics 1990; 78: 100–102. doi:10.1016/S0065-2539(08)60388
12. Binnig and G. Quate. Atomic Force Microscope. *Physical Review Letters* 1986; 56 : 930–933. Bibcode:1986PhRvL..56...930B. doi:10.1103/PhysRevLett.56.930. PMID 10033323
13. Rugar, D. Mamin and H. J. Guethne. Improved fiber-optic interferometer for atomic force microscopy. *Applied Physics Letters* 1989;55 : 2588. Bibcode:1989ApPhL..55.2588R. doi:10.1063/1.101987.
14. M. Birkholz .Thin Film Analysis by X-Ray Scattering. Copyright © 2006 WILEY-VCH Verlag GmbH & Co. KGaA, Weinheim ISBN: 3-527-31052-5.
15. A.Maqsood, K. Khan,M.A. Rehman,M.A.Malik, J. Supercond.Nov.Magn. (2010), doi: 10.1007/s10948-010-0956-9.
16. Agilent Technologies. "Theory on material measurement, operational manual E" Agilent Part No. E4991-90070 (2005).
17. ASTM F394. Standard test method for biaxial flexural strength of ceramic substrates, American Society for Testing Materials (ASTM.org) , Philadelphia, PA, 1991
18. 19 ASTM F394. Standard test method for biaxial flexural strength of ceramic substrates, American Society for Testing Materials (ASTM.org), Philadelphia, PA, 1991

19. Hegazy, A.A. Thermal Joint Conductance of Conforming Rough Surfaces: Effect of Surface Microhardness Variation. Ph.D. Thesis, University of Waterloo, Canada 1985.

CHAPTER 6

Lab Work Performed

All the experimentations were performed in the labs of SCME NUST; most of the work was carried out in the thermal transport laboratory (TTL) and synthesis lab. While Raman characterization were performed at the physics department of UET Lahore, and microwave testing was carried out in MRL UOP Peshawar.

Workload may be divided into three phases

Phase 1 optimization of graphene oxide synthesis

Phase 2 reduction methods of GO

Phase 3 in situ syntheses of cobalt ferrite-graphene composites

6.1. Phase 1: optimization of graphene oxide synthesis

GO is the important precursor to get graphene sheets via wet chemical route, which is further reduced to get RGO sheets, high the quality of GO precursor high quality RGO may be achieved. For composites applications we need high oxidized GO sheets, to achieve high surface area and good dispersion within the composite matrix. We did the numbers of experiments, to get well oxidized GO flakes; finally three methods were evaluated to be the part of this study.

Hummer method

Novel pre-sonication route

Hummer improved method

6.1.2 Hummer Method

Is an efficient way of GO synthesis, but need much attention due to high exothermic step involves in it during water addition to oxidizing mixture, In detail 1 gm graphite flakes taken in a round bottom flask containing 20 ml H_2SO_4 , thoroughly mixed for 10 minutes. 0.5 gm $NaNO_3$ added slowly, while the temperature of the mixture was kept near $0\text{ }^\circ C$ by putting the flask in an ice bath. The temperature of the mixture becomes high due to the addition of 3 gm $KmNO_4$, an ice bath is removed to rise up the temperature up to $35\text{ }^\circ C$, vigorous stirring continued for 30 minutes. 45 ml water added slowly so that rapid increase occurred in temperature, the mixture started boiling and dark bluish color turned into dark brown. The mixture was left to stir for 6 hours continuously, 140 ml water containing drops of H_2O_2 , to stop the reaction. After washing with HCl the mixture was washed thoroughly with deionized water to remove impurities present. Solid GO was obtained by drying in a vacuum oven for 24 hours for further characterizations. The product obtained was named hGO [1].

6.1.2 Novel Pre-sonication Route

Graphite flakes of mass 2 g taken in a 500 ml beaker and 20 ml of acetic acid were added. Sonication was continued for 5 hours at room temperature then washed with deionized water for five times to get neutral pH. Sonicated graphite platelets were dried for 10 hours at 80°C.

Then these sonicated graphite platelets were taken in a flask, and a mixture of H₂SO₄ (30 ml) and nitric acid (10 ml) in a ratio of (3:1) was added and slowly stirred for 1 hour. Potassium permanganate (KMnO₄) of mass 6 g was added to the mixture slowly and vigorously stirred for 1 hour. When the yellow vapors cease, the mixture was diluted with 100 ml warm water and left for 3 days stirring. The yellowish paste obtained was diluted with 200 ml water contains 2 ml hydrogen peroxide (H₂O₂) to stop the reaction. After decantation for 12 hours the cake obtained was washed two times with HCl and thoroughly with distilled water until 7 pH was achieved. The dark brown paste was dried in a vacuum oven for 24 hours to get solid GO which is labeled as nGO for reference.

6.1.3 Hummer Modified Method

In third trail we used the same hummer's reagents with additional KmNO₄ along with changed reactions parameters as reported [2]. The product was referred as mGO. Concentrated H₂SO₄ (30 ml) was taken in a flask contains 1 gm graphite flakes under the ice bath to maintain 0 °C temperature. NaNO₃ (0.5 gm) was added slowly to the mixture, the mixture was allowed to warm up to 20 °C. The reaction was brought up to 50 °C by adding 20 ml water drop by drop. Additional 2 gm KmNO₄ was added after stirring for 1 hour and the reaction mixture was diluted with water (40 ml) and kept stirring for 3 hours at 60 °C. The reaction was stopped by adding 140 ml water contains 30 % H₂O₂ (1 ml).

6.2 Phase 2: Reduction Methods of GO

6.2.1 Reduction by Hydrazine

Reduction of GO with hydrazine hydrate is widely reported [3-5] In detail, GO (100 mg) was well dispersed in 200 ml DI water and the dispersion was vigorously agitated to get homogeneous dispersion throughout the solution. Now 100 ml Hydrazine solution (35 % by weight) was added slowly, the flask was placed in the oil bath and refluxed at 100 °C for 3 hrs. On successful reduction, the brown mixture turned into a dark black suspension. The solution was filtered and washed thoroughly with methanol and water to remove impurities. The solid black filter cake obtained after oven drying was termed as H-RGO.

6.2.2 Reduction by Sodium Borohydride

Sodium borohydride is also used by researchers to reduce the GO [6]. We followed the same procedure with little modification. Water (150 ml) containing dispersed 50 mg dispersed GO, was treated with 15ml NaBH₄ solution (0.1 molar). The mixture was refluxed at 100 °C with vigorous agitation for more than 3 hrs. The black suspension obtained was oven dried to get B-RGO.

6.2.3 Novel Reduction by Sodium Hydroxide

As my literature survey is concerned no trail is reported to reduce GO by using sodium hydroxide. So for the first time we reduce the GO successfully by using a simple and safe route that of sodium hydroxide reduction. NaOH solution (0.1 molar) was added slowly to the beaker contain homogeneous dispersion of 50 mg GO in 150 ml water. The mixture was stirred for 5 hours continuously, while the temperature was kept up to 95 °C throughout the reaction spam. On reaction completion, the product was filtered and thoroughly washed with ethanol and water, solid S-RGO was obtained after drying in oven at 80 °C for 24 hrs.

6.3 Phase 3: In situ Syntheses of Cobalt Ferrites-graphene Composites

Composites of graphene with cobalt ferrites were synthesized by in situ Co-precipitation mechanism [7]. In typical method 0.02 mol of Fe (NO₃)₃.9H₂O salt along with 0.1 mol Co (NO₃)₂.6H₂O was added to 200 ml DI water and mixed to form homogeneous solution. Appropriate amount of GO was mixed with 4 gm NaOH to achieve the GO loading up to 0 % , 0.1 % , 0.5 % and 1 % with compare to ferrites salts precursors. Ferrites- salt containing mixture was heated up to 90 °C and stirred vigorously, while NaOH contain GO was added drop by drop. The one pot mixture was left for 3 hours stirring without lowering the temperature. The precipitate formed was filtered and washed thoroughly with water until we got neutral pH. Powder obtained was dried in oven and ground with the motor and pestle, the sintered for 3 hrs at 800 °C in the furnace. Sintered samples were named S₀, S₁, S₂ and S₃ respectively.

References

1. W. S. Hummers. Hoffman Preparation of graphite oxide. *J. Am. Chem.Soc.* 1958; 80: 1339.
2. D. C. Marcano, D. V. Kosynkin, J. M. Berlin, A. Sinitskii, Z. Sun, A. Slesarev, L. B. Alemany, Wei Lu, and J M. Tour. Improved Synthesis of Graphene Oxide Received for review. *ACS NANO* 2010.
3. K. moon, J. Lee, Rodney s. Ruoff And H. Lee. Reduced graphene oxide by chemical graphitization *NATURE COMMUNICATIONS* 2010; 10:1038.
4. G.K.Wang et al. Facile synthesis and characterization of graphene nanosheets. *J. Phys. Chem* 2008; 112:8192–8195.
5. Gao, W. Alemany, L. B. Ci, L. and P. M. Ajayan. New insights into the structure and reduction of graphite oxide. *Nat. Chem.* 2009; 1:403–408.
6. S. Park, C.W. Bielawski and R. S. Ruoff. The chemistry of graphene oxide Daniel R. Dreyer. *Chem.Soc.Rev* 2010; 39: 228–240.
7. H. Gul, A.Maqsood. Structural, magnetic and electrical properties of cobalt ferrites Prepared by the sol-gel route. *Journal of Alloys and Compounds*, 465 (1-2): 227-231, 2008.

CHAPTER 7

Results and Discussion

7.1 XRD Characterization

7.1.1 Oxidation of Graphite

In Fig. 7.1, XRD spectra are shown for the starting material (graphite) and GO samples. For graphite, two sharp peaks are seen in the pattern, the principal peak at 26 degrees and a minor peak at 54 degrees confirms graphite spectra [1].

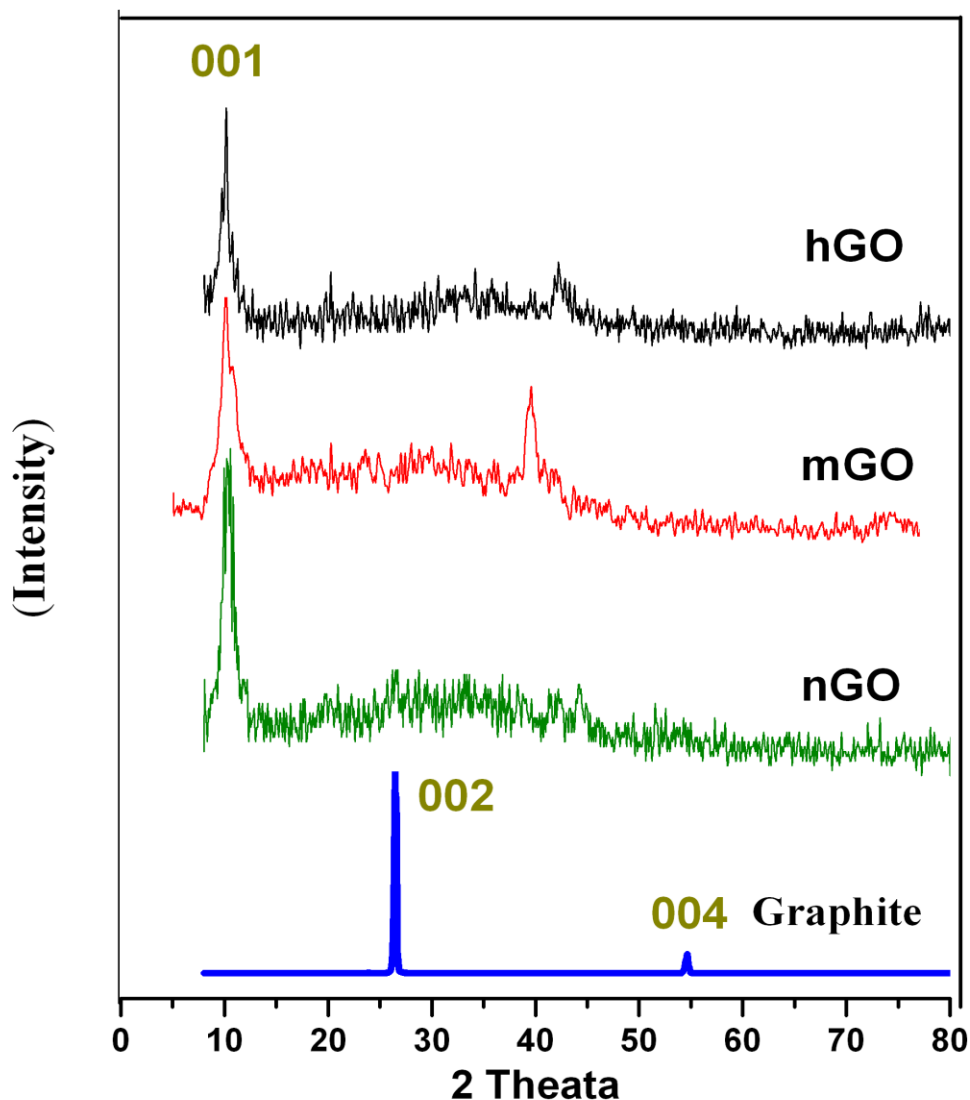


Figure 7.1 XRD spectra of all the three GO samples taken in bulk powder form in 2 theta range from 8 to 80 degrees.

The sharp peak at 11 degrees in hGO spectrum corresponds to (001) plane in the interlayer distance of 6.7\AA , and the small peak at 40 degrees shows the graphite portion remaining in the final product of GO, showing the incomplete oxidation. Furthermore, the GO spectrum for modified synthesis routes also shows the same results as for hGO, but with lower intensity peak at 11 degrees and higher intensity peak at 40 degrees. It shows less efficient oxidation compared to the Hammer

method (mGO). High intensity single peak at 11 2θ confirms successful oxidation of graphite into GO for novel synthesis route (nGO) [2-3].

7.1.2 Reduction of GO

XRD for all the three reduction routes are shown in figure 7.2. It has revealed that broadening occurs in (002) plane of GO due to reduction in periodicity of graphite structure of the RGO.

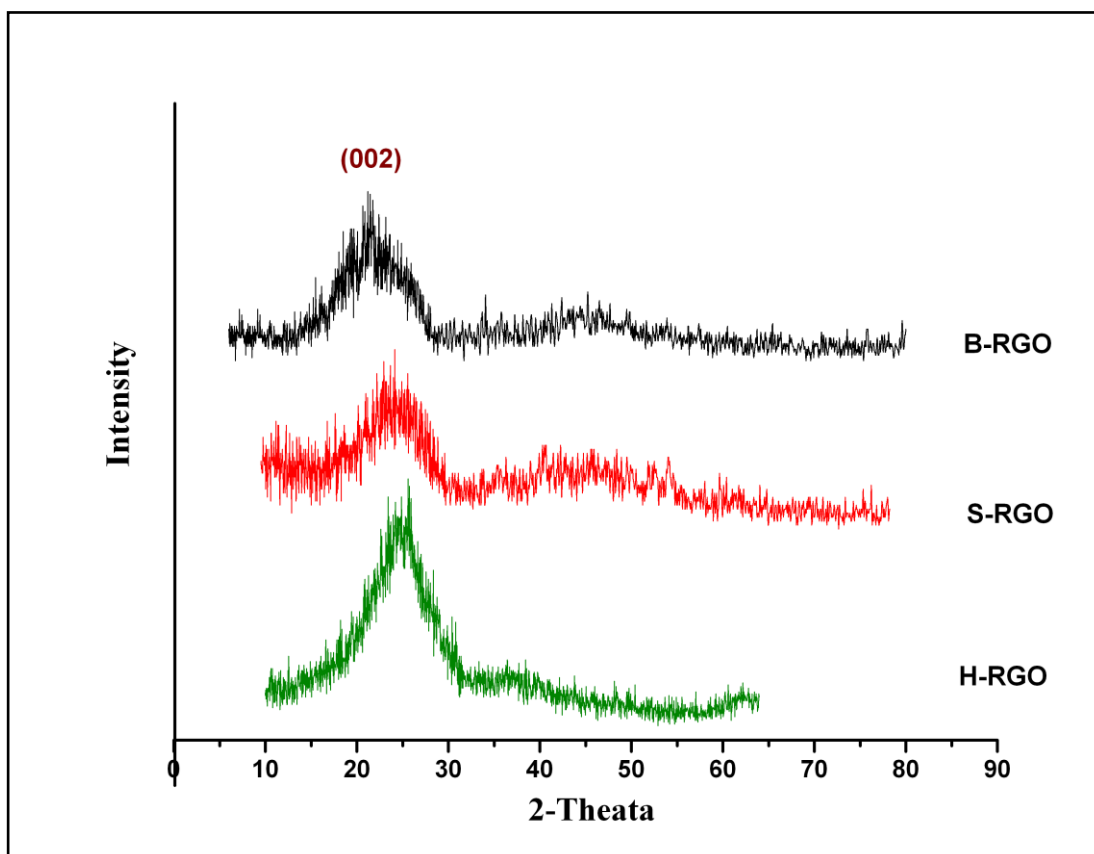


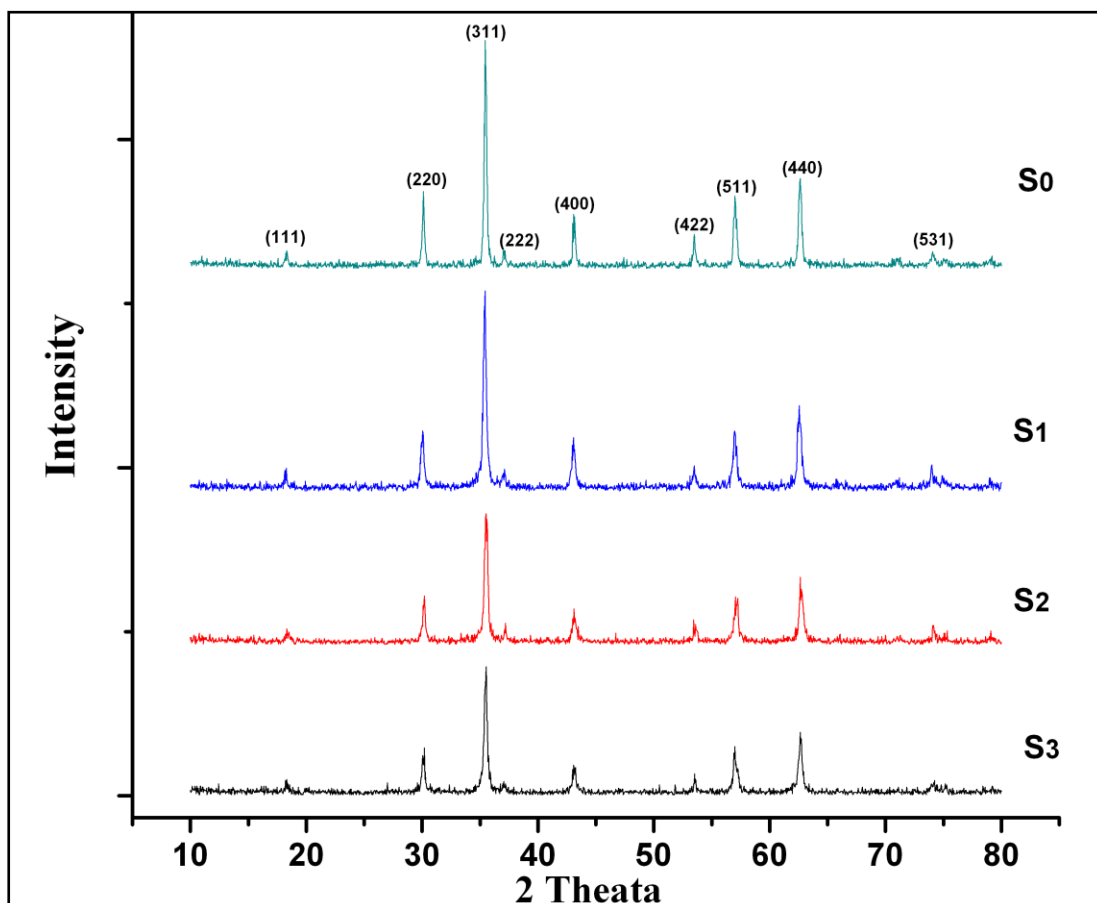
Figure 7.2 XRD spectra of all three RGO samples

After reduction of nGO samples the peak shifts toward the right and broadening occurs due to impurity and inhomogeneity of the samples. For the sample reduced with hydrazine, we got relatively sharp peak within the range between 20 and 30 degrees and are the evidence for efficient reduction compared to others two reduction routes. Moreover a single hump achieved in the 20 to 30 degrees for all the three samples, which reflects a successful reduction as reported [4].

7.1.3 Phase Analysis of Composites

The ferrite powder obtained was sintered at 800 °C for 3 hours in a furnace, and then analyzed by X-ray diffraction instrument to get the characteristic spectra for all the prepared samples, as shown in figure. 7.3. For these samples characteristic planes

(111), (220), (311), (222), (400), (422), (511), (440), and (531) are observed in all the samples. And these planes correspond to pure crystalline phase of cobalt ferrites matched with reference card no (JCPDS, 03-0867) of XRD. High intensity with



respect to background signals and sharpness of these characteristic peaks is the evidence for good quality crystalline cobalt ferrite formation.

Figure 7.3 XRD spectra for cobalt ferrites and its composite samples with Graphene

As we can see that impurity phase is present only for 1 % doping of graphene into cobalt ferrites at 28 degrees, so for other samples 0.1 and 0.5 % doping, graphene amount is not enough to be visible in XRD spectra [5-6].

7.2 FTIR Analysis

7.2.1 Functional Group Analysis of GO

The FTIR spectra for all GO samples were obtained in frequency ranges from 1000 cm^{-1} to 4000 cm^{-1} , Shown in Fig.7.4. The powder samples were mixed with KBr and pressed in the form of pellets and heated for 1 hour at 60 $^{\circ}\text{C}$, to dry these pellets before FTIR analysis.

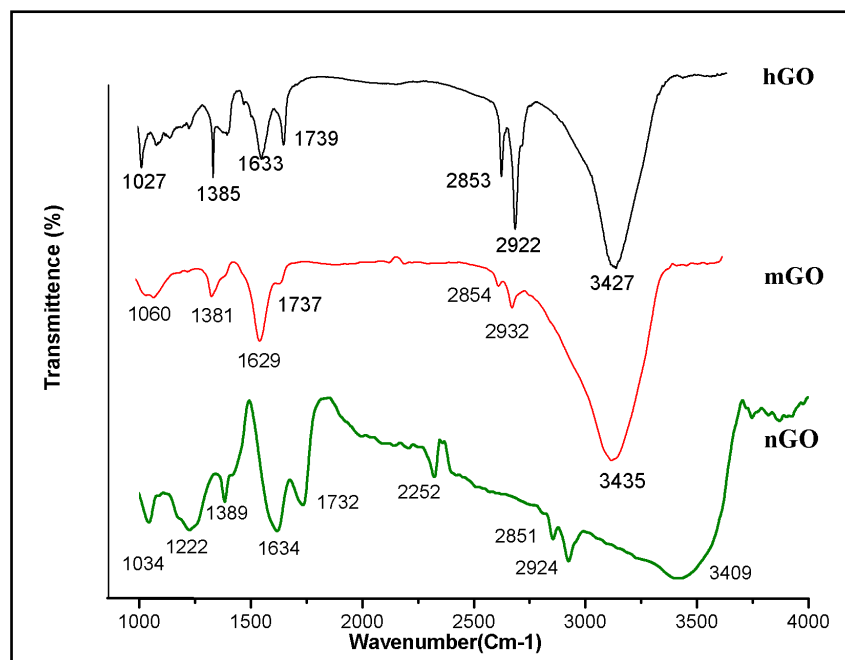


Figure 7.4 FTIR of three GO samples taken with KBr pellets in a range from 1000 cm^{-1} to 4000 cm^{-1}

The broad peak beyond 3000 cm^{-1} attributes to O-H stretching vibration, the small peak at 1740 cm^{-1} shows C=O group, the C-H stretching appears at two peaks at 2851 cm^{-1} and 2924 cm^{-1} , and peak at 1389 cm^{-1} refers to C-N stretching, while 1034 cm^{-1} peak attributes to C-N stretching. Is also clear from XRD, here in FTIR we have relatively more absorption of C=O and C-H along with broader peak of OH stretching for nGO sample and hence is the evidence for efficient oxidation. All these peaks are characteristics of GO [32-35]. We experienced one new absorption band for nGO samples which is the characteristic absorption for nitrogen attachment due to treating the graphite with NH_3 , in this synthesis mechanism [7].

7.2.2 Groups Present in RGO Samples

We performed FTIR analysis of reduced samples, to see the effect of reduction in the product. Here from the FTIR spectra of three different types of reduction routes, we may conclude that after reduction most of the peaks suppressed, while some completely diminished as shown in Figure 7.5. The absorption broad peak after 3000 cm^{-1} , is still dominantly present in all the reduced samples which are the evidence that some O-H groups along with incorporated water molecule are still there in the RGO samples [8].

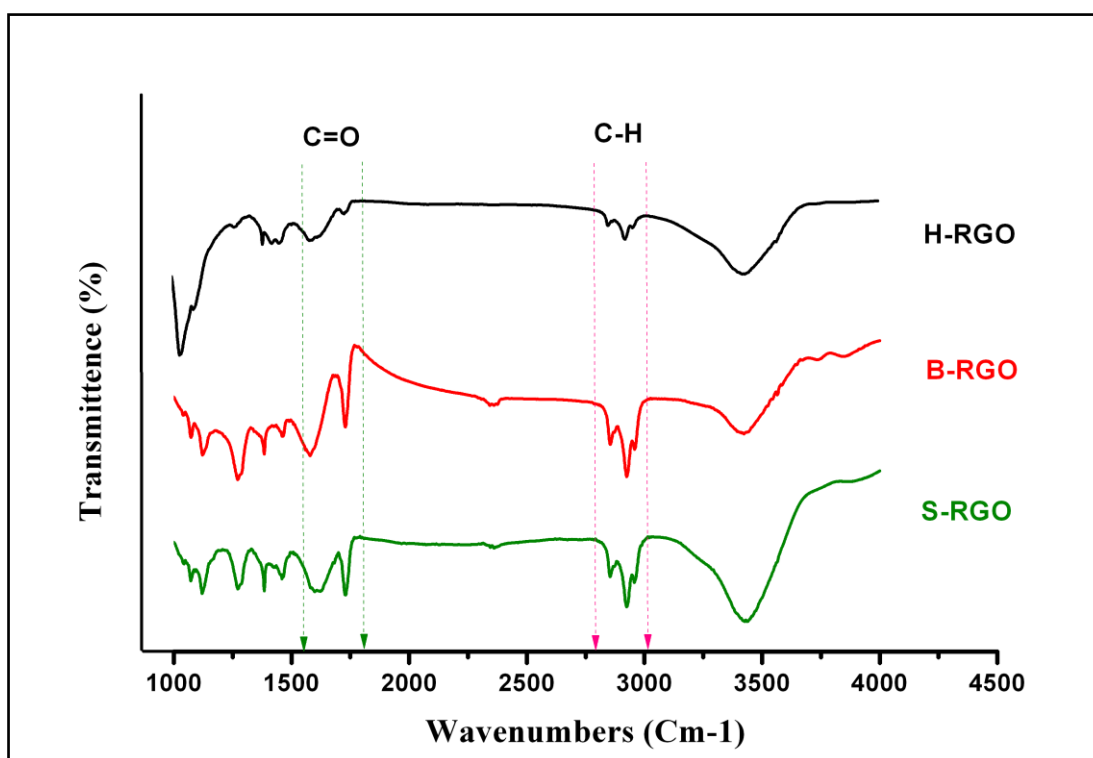


Figure 7.5 FTIR spectra of RGO samples

To compare the results of different reducing agents, it is seen from the Figure 7.5, that all the peaks of H-RGO, except beyond 3000 cm^{-1} are of very low intensity compared to other two routes. There are only two prominent absorption bands retained after reduction, which are attributed to O-H and C-O stretching, this is the proof of successful recovery of graphene Skelton which is also confirmed by XRD. The same case is for S-RGO and B-RGO samples but with the relatively lower suppression of GO characteristic peaks which is an evidence for weak reduction by these two routes [9].

7.2.3 FTIR Analysis of Cobalt Ferrites and its Composites

FTIR spectra are shown for cobalt ferrites as well as for three composite samples in Figure 7.6. It is clearly shown that there are only two characteristic peaks at 425 cm^{-1} and 590 cm^{-1} along with a broad downhill after 3000 cm^{-1} for S0 sample. Peak at 425 cm^{-1} attributes to Fe-O group and 590 cm^{-1} peak is due to the presence of Co-O group, while broad peak after 300 cm^{-1} is due to incorporated water molecules. For composite samples we have extra peaks at $1380\text{-}1390\text{ cm}^{-1}$, $1620\text{-}1680\text{ cm}^{-1}$ and at $2920\text{-}2930\text{ cm}^{-1}$ attributes to C-H, C=C and C-H₂ deformation respectively. All this data is in agreement with literature for cobalt ferrite formation as well as graphene-cobalt ferrites composites [10-11].

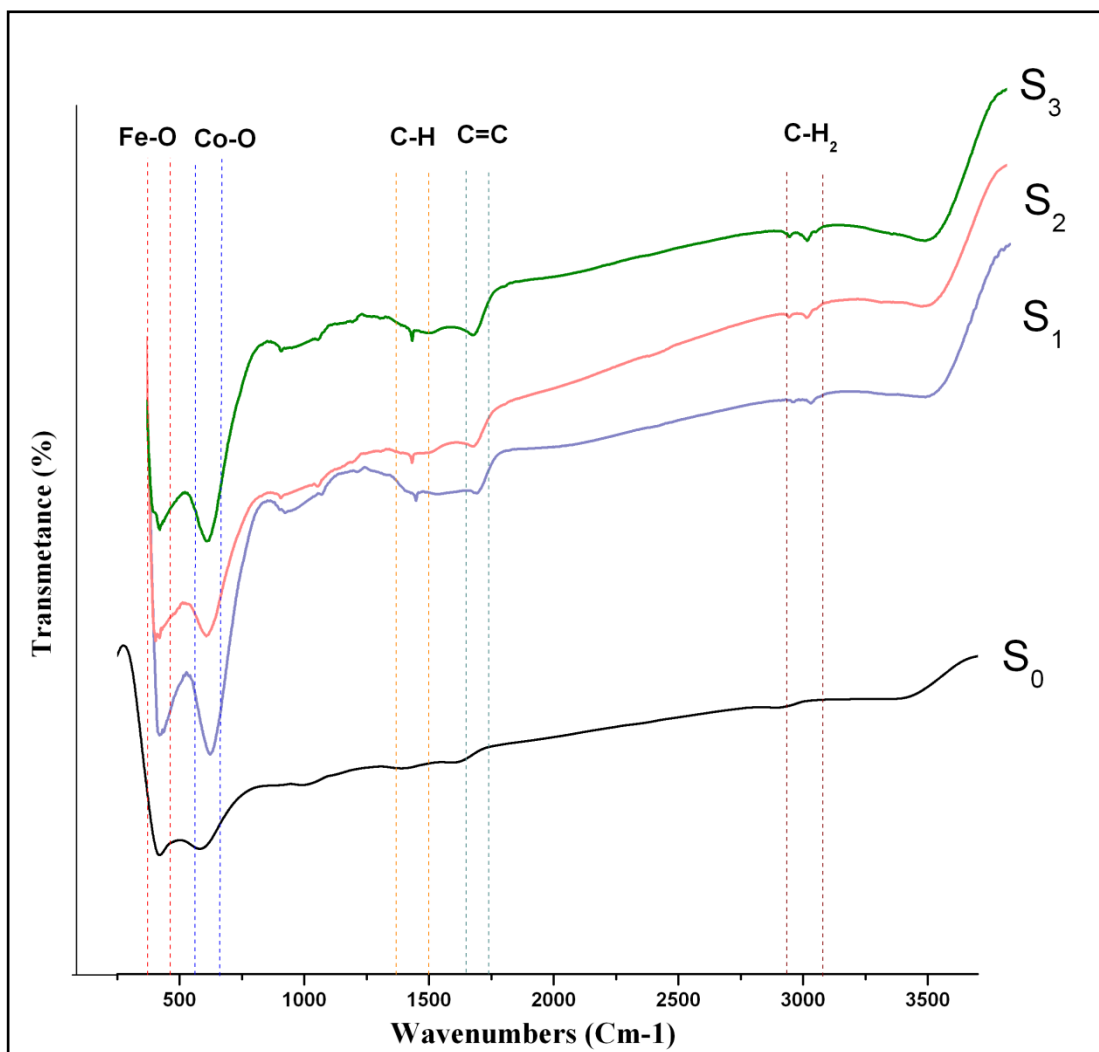


Figure 7.6 FTIR for cobalt ferrites and its composites samples with different Percent loading of graphene

7.3 Raman Spectroscopy

7.3.1 Raman Spectra of GO Samples

Raman scattering for all GO samples are shown here in form of D and G peaks in figure 7.6. Raman analysis was performed by Lab RAM 800HR, made HORIBA, in the range of 1100 cm⁻¹ to 2800 cm⁻¹ shown in Fig.3. The spectrum impart two pronounced features of GO at 1330-1350 cm⁻¹ and 1570-1590 cm⁻¹, which are referred to D and G bands, consequently. The D band is due to the structural imperfections caused by the hankering of OH and epoxy groups on the basal plane of carbon. The G band is the evidence of the sp³ and sp² hybridization, due to distortion in the crystal structure of the carbon atoms results from oxidation. Relatively short FWHM and nearly same intensity of both the peaks, shown in table 1, reveal that GO flakes obtained are mostly monolayer as illustrated previously [12-13]

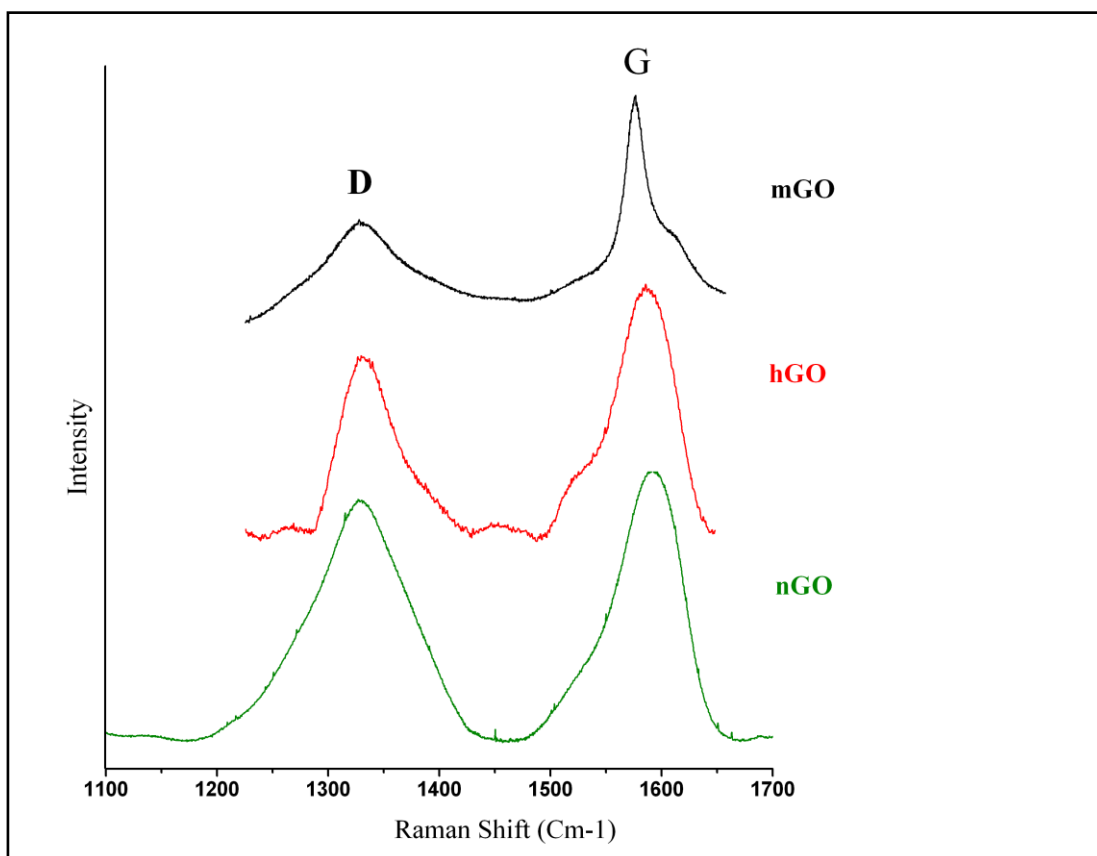


Figure 7.7 Raman Spectroscopy spectra for all the three GO samples taken on silica substrate

The detail of these characteristics peak is given in table 7.1, along with its intensity ratio. For all GO samples the D and G bands position are the same refers to GO structure, but intensity is considerably increased from mGO to nGO. The intensity ratio of D versus G is most important parameter to measure the level of oxidation of carbon derivatives. Here we have shown that as we go from graphite to nGO samples the intensity ratio increases reached up to 0.89 which is the evidence for monolayer GO as reported [14-15]

S.NO	Sample	D			G			I _D /I _G
		position	Ht	FWHM	Position	Ht	FWHM	
1	Graphite	1350	650	25	1575	2950	10	0.42
3	mGO	1331	8947	75	1573	15654	38	0.57
2	hGO	1336	5648	57	1586	7802	60	0.72
4	nGO	1328	25037	90	1588	28122	67	0.89

Table 1 shows the position and intensity of all GO peaks and its intensity ratio.

7.4 Size, Morphology and Topography

7.4.1 SEM and AFM of GO samples

In figure 7.9 SEM micrographs of all the three samples (hGO, mGO and nGO), are shown. For hGO samples we have sheet like morphology up to seven micro meter lateral size, also having a low thickness as no considerable height is shown from the micrograph. Similar results are obtained for nGO samples but with the small lateral size and having a smooth sheet like morphology.

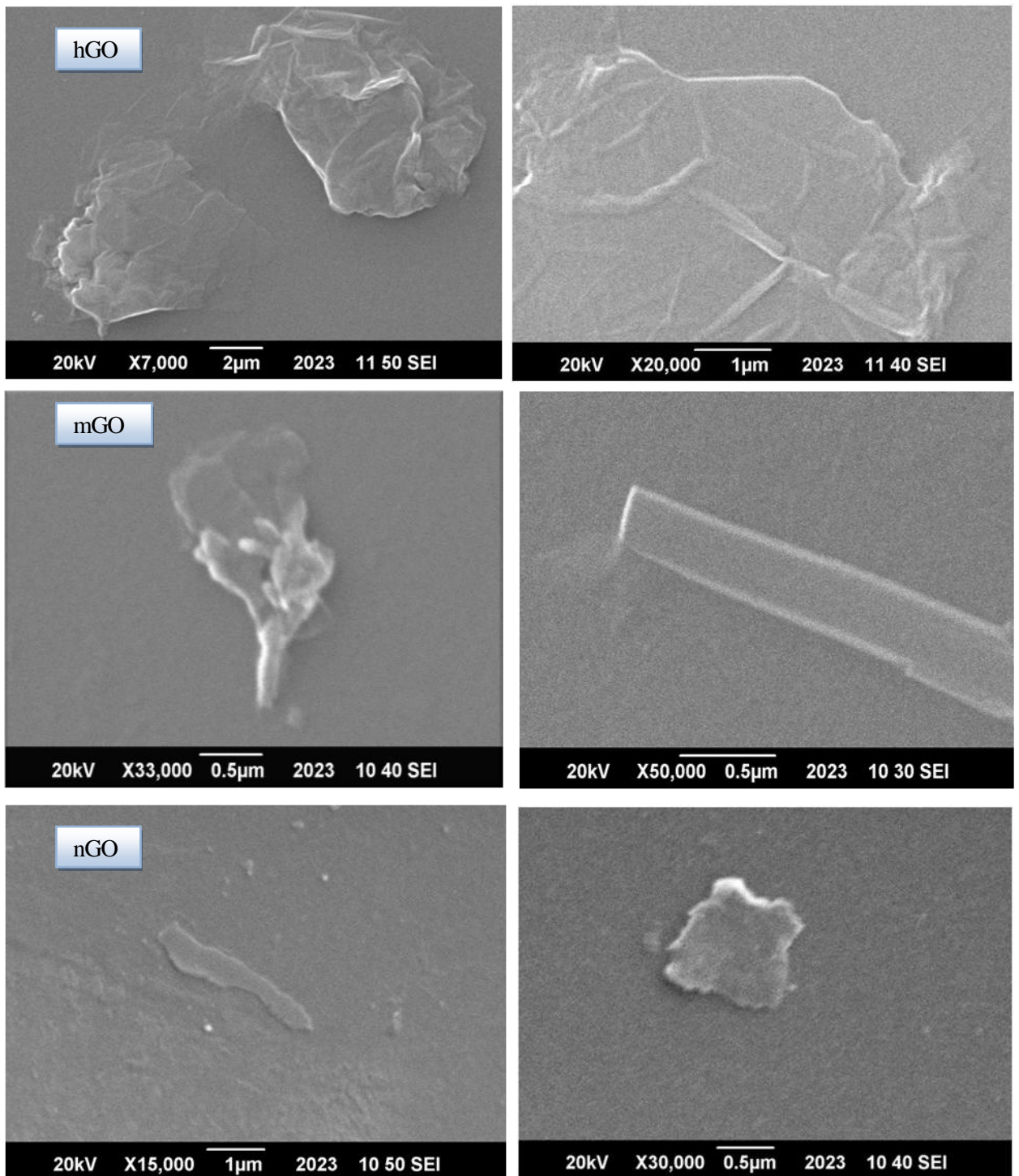


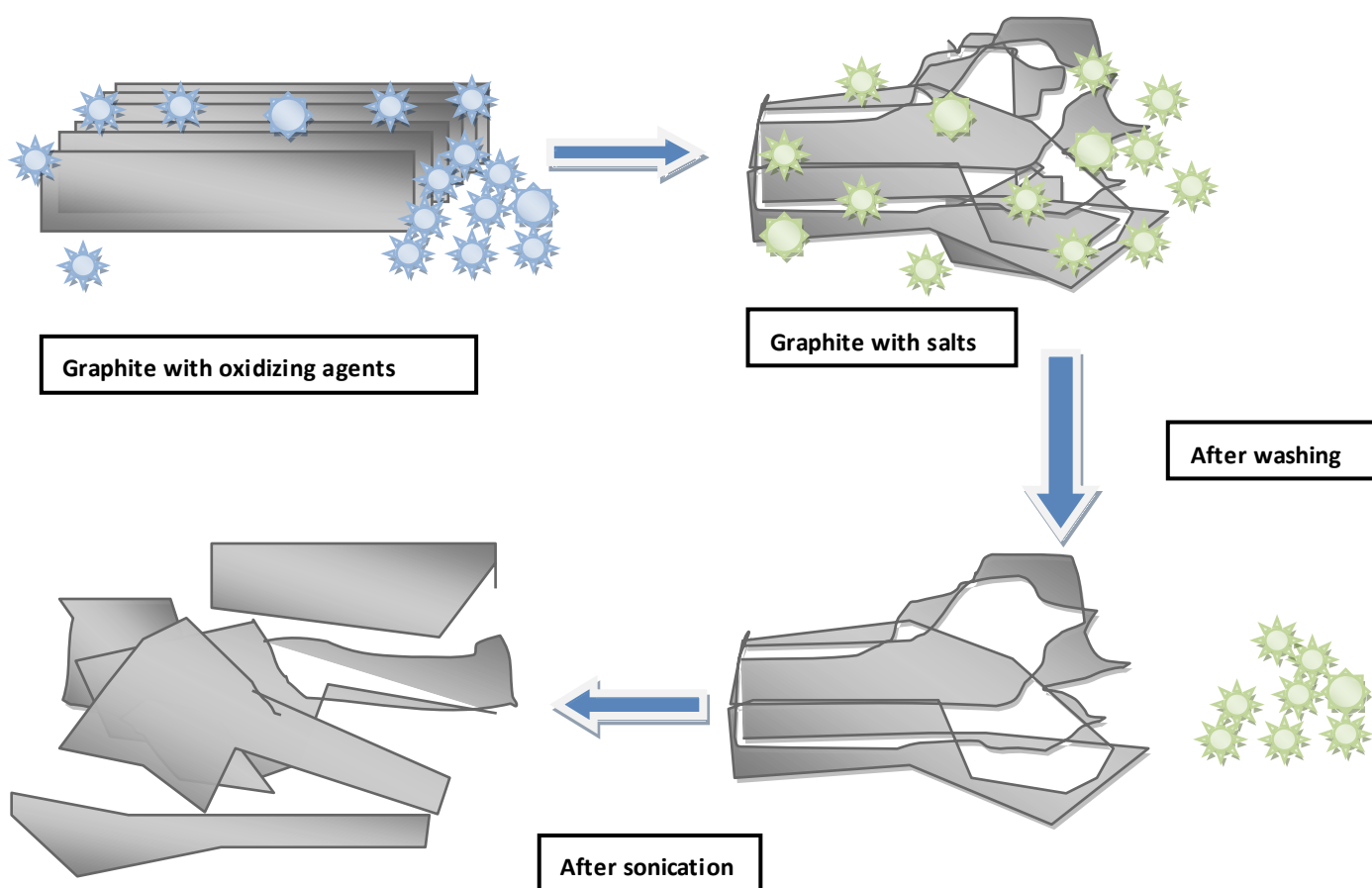
Figure 7.8 SEM micrographs of GO samples left side are at low magnification while right side images are at high magnifications

The modified synthesis route has interesting ribbon and flower like morphology. It is clearly suggesting that the nGO have flowers like morphology along with elongated stems, which is divided and dispersed separately on sonication. SEM results are further confirmed by AFM images as shown in figure 7.10-7.12. In AFM images we

individually dispersed GO flakes for both hGO and nGO of sheet thickness up to 0.6 nm and hence referred to mono layer GO flakes as reported [16-17].

On the other hand mGO samples have sheet and ribbons like morphology having thickness --- nm for sheet and –nm for ribbons. Hence it may be concluded that for nGO and hGO samples we have high oxidation of graphite precursors while for mGO the precursor is not fully oxidized , that's why we get amazing morphology like flowers with ribbons as stem. The reason behind is, that the ends of graphite flakes are attacked by oxidizing agents and started opening but the opening processes of these sheets into single or bi layers were not completed and hence we got flower like morphology composed of multi layer GO flakes, also revealed from the oxidation quality of XRD spectra for all the three samples..

The suggested scheme model is given here.



AFM images of GO samples

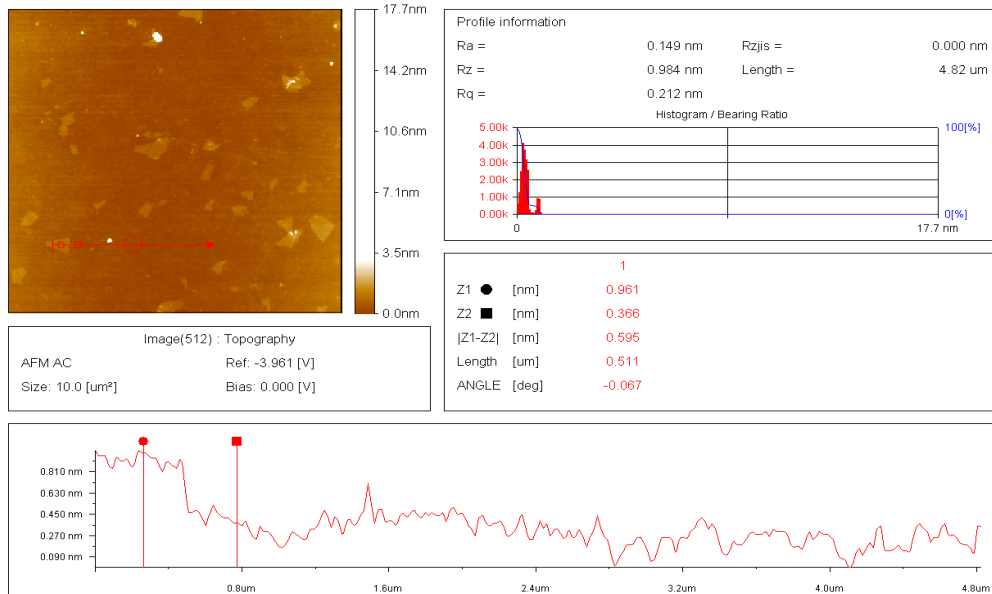


Figure 7.9 AFM image of nGO on silica substrate at tapping mode scanning

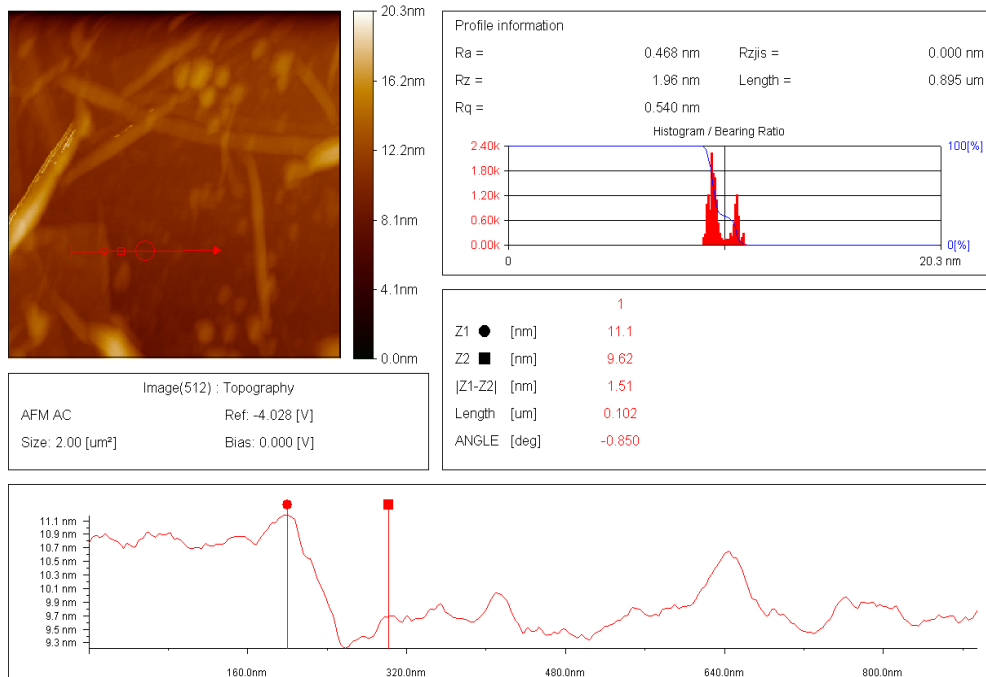


Figure 7.10 AFM image of mGO on silica substrate at tapping mode scanning

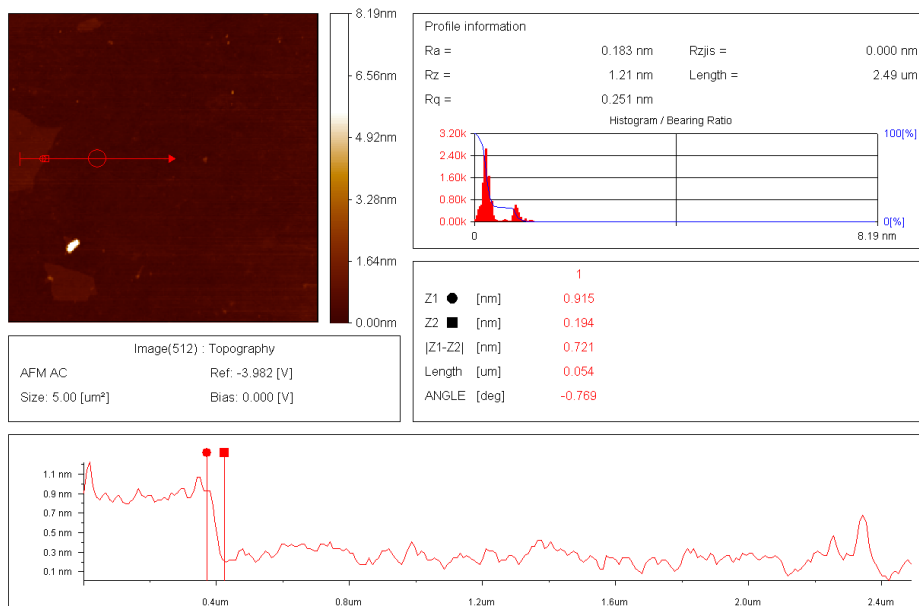


Figure 7.11 AFM image of hGO on silica substrate at tapping mode scanning

7.4.2 SEM of RGO Samples

The SEM images were taken in bulk form of reduced graphene oxide samples as

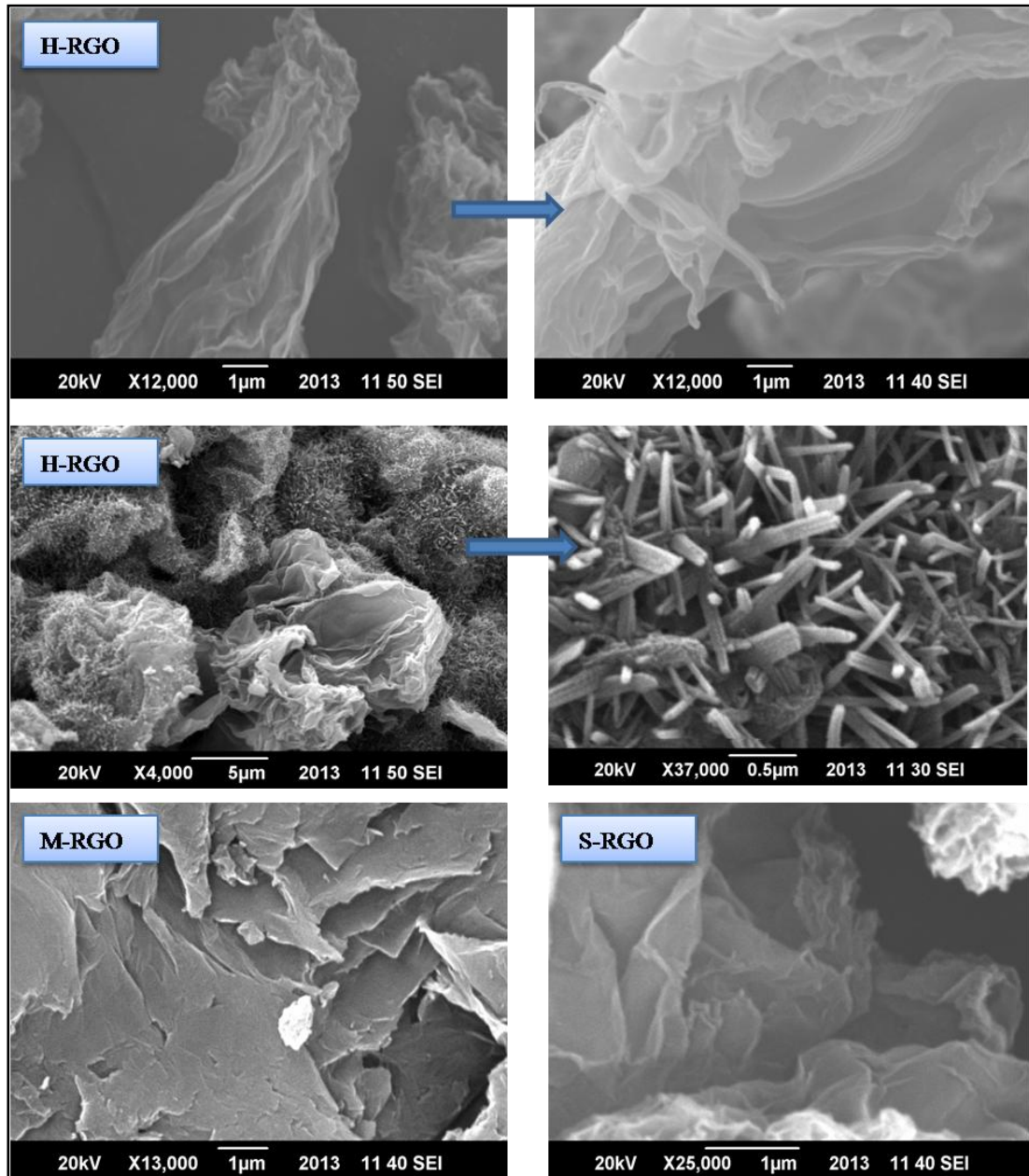


Figure 7.12 SEM micrographs of RGO samples taking from powder sample o carbon tape

shown in figure 7.13. First two images are , of H-RGO sample, with hGO precursor.

After reduction the sheet like morphology is wrinkled and got the shape of crumpled paper. This wrinkling after reducing GO sample is possibly due to the high lateral size and low thickness of GO precursor. We also investigated the mGO sample after

hydrazene reduction, and we got the same flower like morphology , but here after reduction theses graphene flowers are more dominant. We have seen here an area consists of an accumulation of graphene ribbons, and is the evidence to strengthen the claim for this morphology before reduction.

7.4.3 SEM of Ferrites and its Composites Samples

Figure 7.14 shows the micrographs of cobalt nano particles (S_0) synthesized by co-precipitation technique and all the three samples (S1, S2, S3) respectively. S_0 sample was analyzed via making suspension in water without sonication, and hence we see the cobalt ferrite particles up to 15 nm by size, along with agglomeration of these particles in the form of an island.

The composite samples were analyzed by SEM in bulk-powder form putting on the clean glass substrate. As shown from figure- that for very low concentration (0.1%), there is no graphene flake to see within cobalt ferrites, while for another two samples S2 (0.5%) and S3 (1%) we have graphene flakes embedded with in cobalt ferrites.

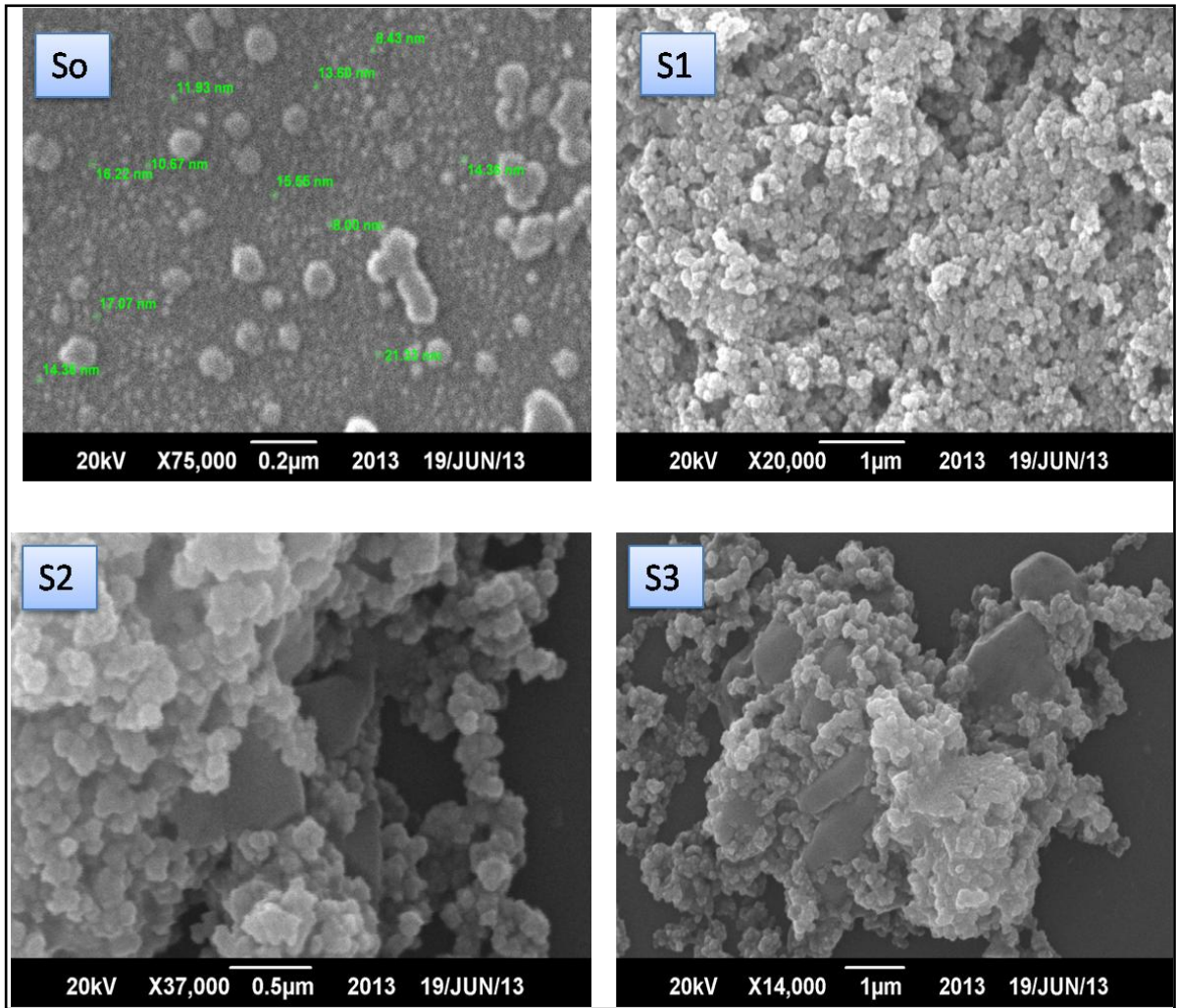


Figure 7.13 SEM images of cobalt ferrites and graphene based composites

7.5 Electrical Characterization

The microwave composed of two perpendicular magnetic and electrical vectors [18], as shown in figure 7.15.

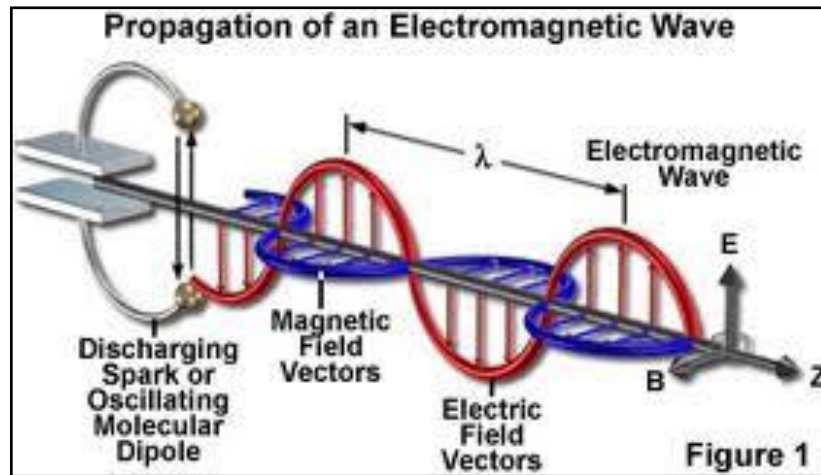


Figure 7.14 Demonstration of electromagnetic wave

So efficient absorption can only be achieved by canceling both the electrical and magnetic components of it. When we use some media for microwave absorption, it should be capable of opposing both these perpendicular vectors. Here we want to study the absorption of microwave by incorporating electrically conducting graphene sheets into magnetic (cobalt ferrites) matrix.

7.5.1 Real permittivity and Permeability

The behavior of frequency dependence of the real parts (ϵ' and μ') of permittivity and permeability for cobalt ferrites (S_0) and its composites with different loading of graphene (S_1, S_2, S_3) at room temperature is shown in figure 7.16. As is clear from this study that all the samples exhibit frequency dependency for both permittivity and permeability in the low frequency range which become independent of frequency at higher frequency and shows consent behavior with respect to it. The variation of ϵ' with respect to change in composition may be explained by Maxwell-Wagner theory of space charge polarization [15]. Due to the inhomogeneous structure composed of good conducting grains and poor conducting grain boundaries of dielectric materials space polarization occurs. In more detail the electrons are approaching to the grain boundaries passing through the conducting media within the grain by hopping, piled up along the boundary lines and produced polarization [19].

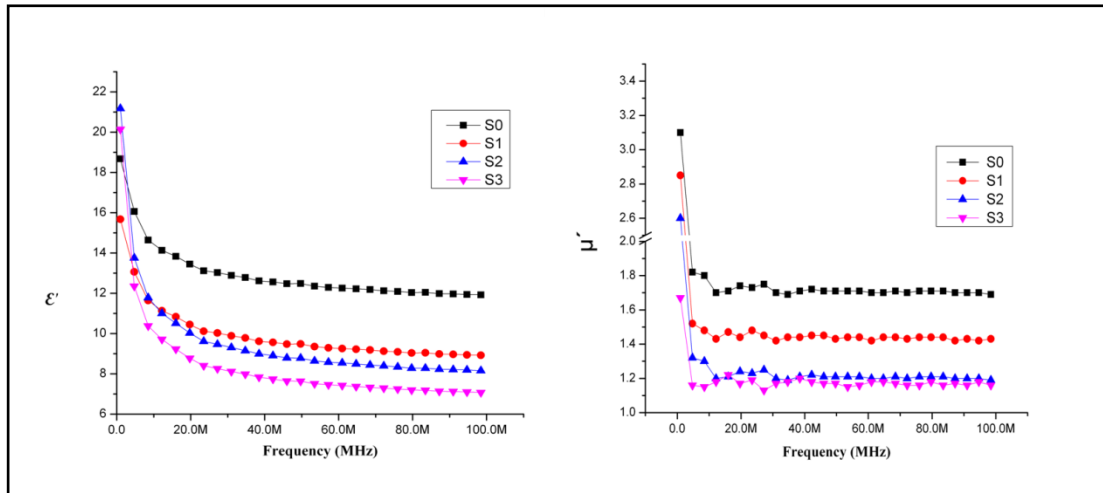


Figure 7.15 Real part of permittivity and permeability of Co nanoferrites and composites samples in the frequency range of 1MHz to 100MHz.

When the applied field frequency is increased the probability of electron approaching towards grain boundaries decreases and hence dielectric constant also goes down. For composite samples the lower curves are due to the conducting graphene sheets in between the cobalt ferrite particles, which tend to decrease polarization due to conduction of charges along these conducting sheets.

7.5.2 Complex Permittivity and Permeability

Complex spectra for permittivity and permeability are taken for all the composites and pure cobalt ferrites samples in the frequency range up to 100 MHz are shown in Figure 7.17. Both imaginary parts of permittivity and permeability refer to the energy loss from the material to the electric and magnetic field respectively [20]. For permittivity the complex portion is highly dependent on the frequency of all the four samples and decrease rapidly with increasing frequency which becomes less dependent after 50 MHz if we compare the response of cobalt ferrites to its composite samples, it can be seen from the Figure 7.16. That at the start composites samples has higher loss than the pure ferrites while going at higher frequency the loss became higher for ferrite sample comparable to all other composites. Although there is some gap in the response of ferrites and composite samples but it is negligible and hence we can assume that no major affect is there in ferrites loss to electric field due to graphene incorporation. This decrease may be due to the presence of comparatively low magnetic and dielectric graphene sheets [21]. Considering the spectra of complex permeability with respect to frequency as shown in figure 7.16 b. We have some oscillating response from the zero mean point at lower MHz for all the composite samples which became stagnant at higher frequency. While cobalt ferrite has some rapid decrease and then became independent of higher frequency. The oscillatory response of composites is due to the presence of ferromagnetic nature of graphene sheet in cobalt ferrite matrix, at the start due to low incident frequency the magnetic field is not reflected hence negative values are recorded for loss of magnetic field by the samples. At higher frequency the ferrite response is dominated

and goes up to some higher value then comes down and became linear in further frequency range. But again the overall response to magnetic loss is the same for all the four samples.

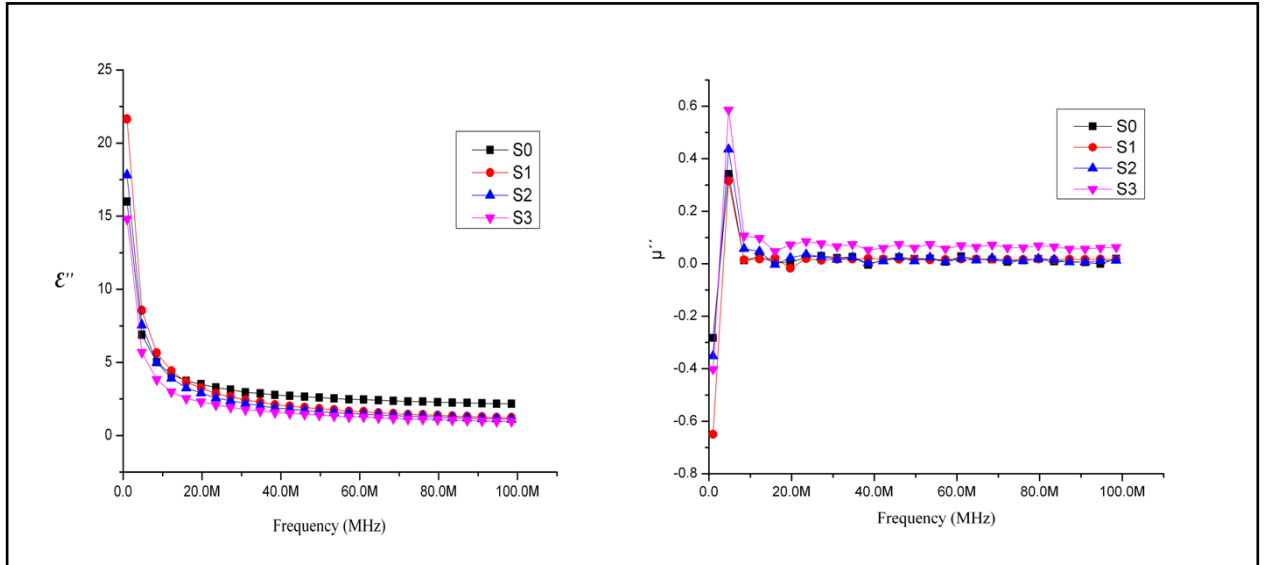


Figure 7.16 complex parts of permittivity and permeability of Co nanoferrites and composite samples in the frequency range of 1MHz to 100MHz.

7.5.3 Microwave Absorption

The reflectivity curves in the frequency range up to 3 GHz for RGO and cobalt ferrite samples are shown in Figure 7.18 and 7.19, with nearly equal thickness (1.9 ± 0.1 mm). Maximum absorption peak is reached at nearly 250 MHz at the value up to 9 db, while for ferrites we have greater absorption peak up to 13 db at very higher frequency (2GHz). Absorption spectra of composites samples are shown in figure 7.18. It is clear that the position and value of absorption peak is not much displaced due to less percent doping of graphene (1 %), but is very interesting that parent cobalt ferrite absorption peak is changed in to a band of small peaks of nearly equal values. Moreover as the doping of graphene is increased this band became wider. The reason behind is that single point maxima is converted to band of noise due to inhomogeneity and combine effects of electric (due to graphene), and magnetic dielectric nature (due to cobalt ferrites). So it is finally concluded that graphene based cobalt ferrites composites may be a potential candidate for microwave shielding.

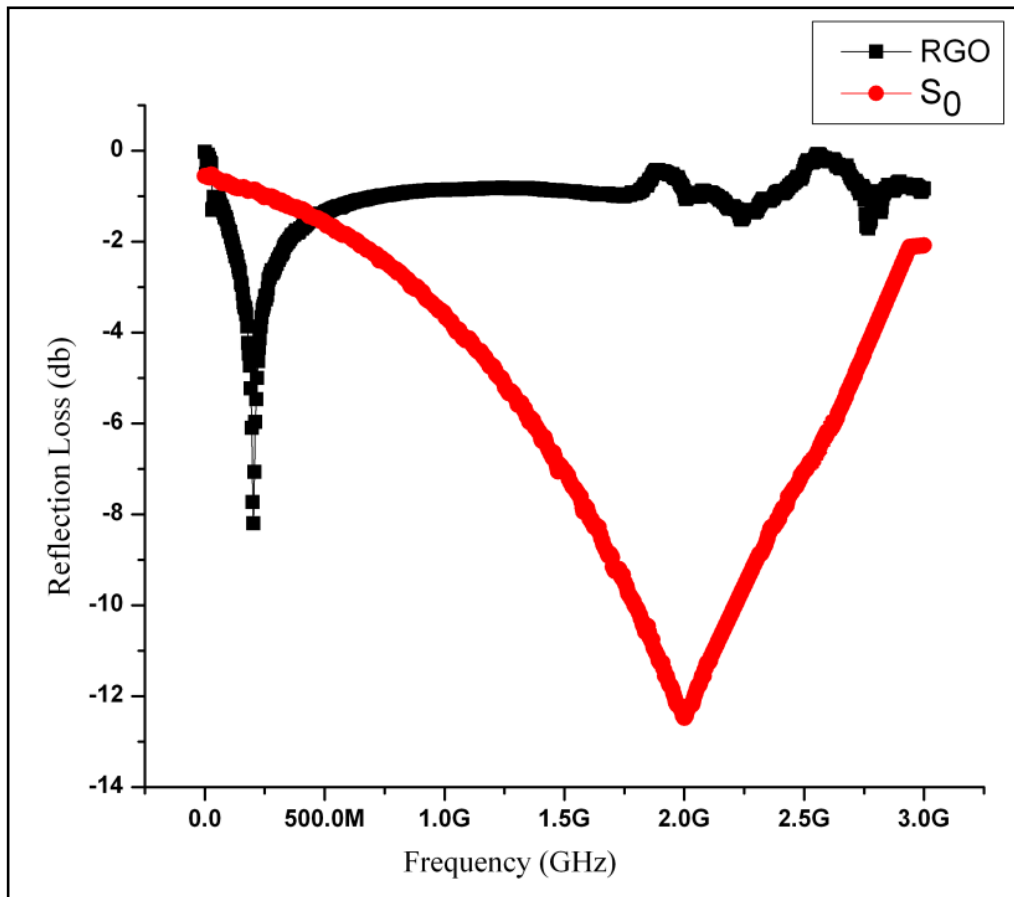


Figure 7.17 Microwave absorption curves of cobalt and RGO samples with thickness 1.9 ± 0.1 mm

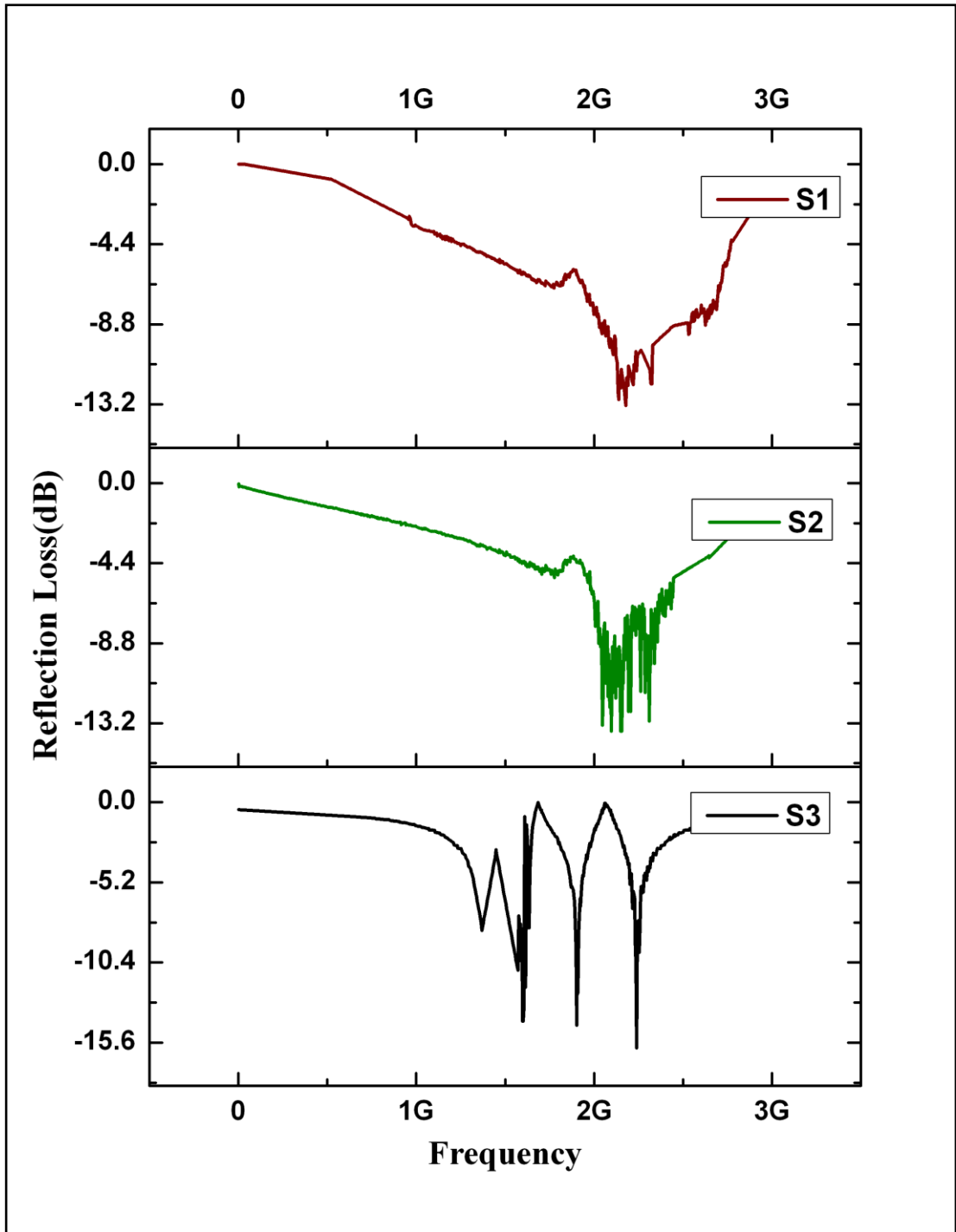


Figure 7.18 Microwave absorption curves of Co composites samples with thickness $1.9 \pm 0.1 \text{ mm}$

7.6 Mechanical Characterization

7.6.1 Stress versus Strain Behavior

Stress versus strain curves are given for all the composites and RGO sample are given in figure no 7.20, As the loading of graphene in cobalt ferrites is very low (up to 1 %), so all the composite samples behave like ceramics as reported for ferrites samples [22]. While for RGO, the deformation behavior is somehow like poor polymer as shown in Figure 7.20. This behavior is much expected from the RGO sample as it has a flaky morphology along with flexible nature. Further it is clear from the figure... that time before failure is much increased by increasing the percent loading of graphene in cobalt ferrite matrix. The UTS for all the samples and RGO is given in the table 7.1.

From the UTS data analysis it is revealed that the overall strength of composites is improved by doping of graphene in the cobalt ferrites sample.

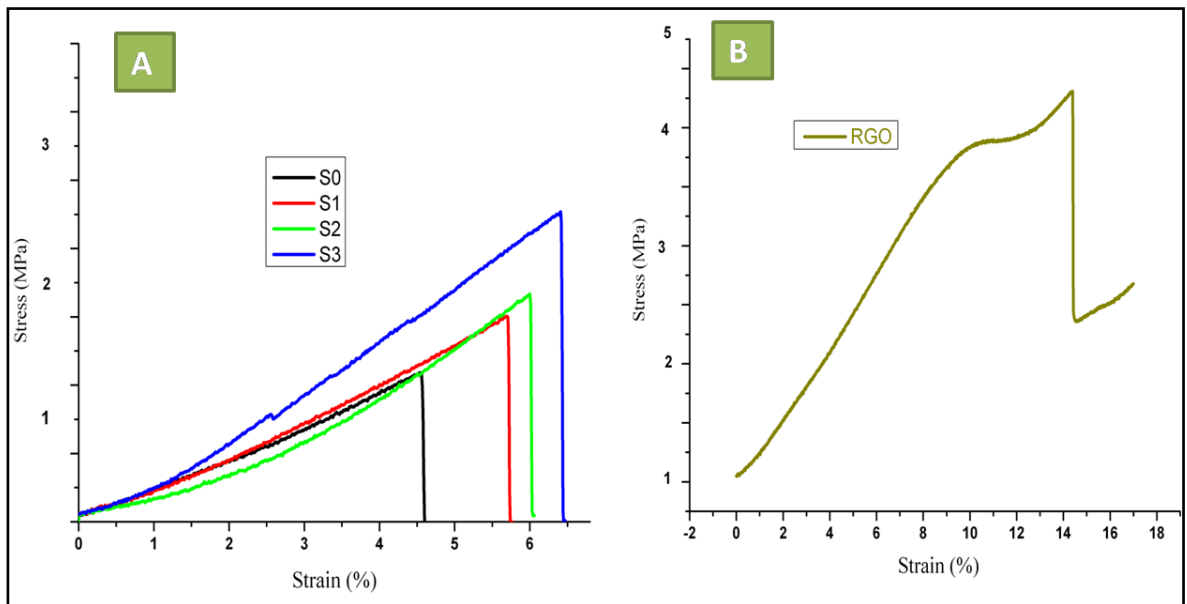


Figure 7.19 stress strain curves for composites and RGO samples

7.6.2 Toughness

In this study our aim was to improve the toughness of the ferritic material by the addition of graphene to it. So here we evaluated the overall relative toughness of our samples by a simple method. As the overall toughness of the material can be measured by calculating the area under the stress strain curve. So all these areas are calculated via origin approximation and compared with each others. Relative toughness versus graphene loading to cobalt ferrites are illustrated here in the form of bar graph is shown in figure 7.21.

It can be seen from the graph that ferrites having strong brittle nature with very low toughness up to $10,000 \text{ J/m}^3$ which increased up to $32,000 \text{ J/m}^3$ by only 1 % graphene addition. We got very high toughness up to $63,000 \text{ J/m}^3$ for RGO sample.

So it is revealed from this experimental data that there is surely a possibility to improve the toughness of cobalt ferrites by doping with graphene, which may lead to solutions for problems such as achieving flexible devices of ferrites composites for different microwave applications.

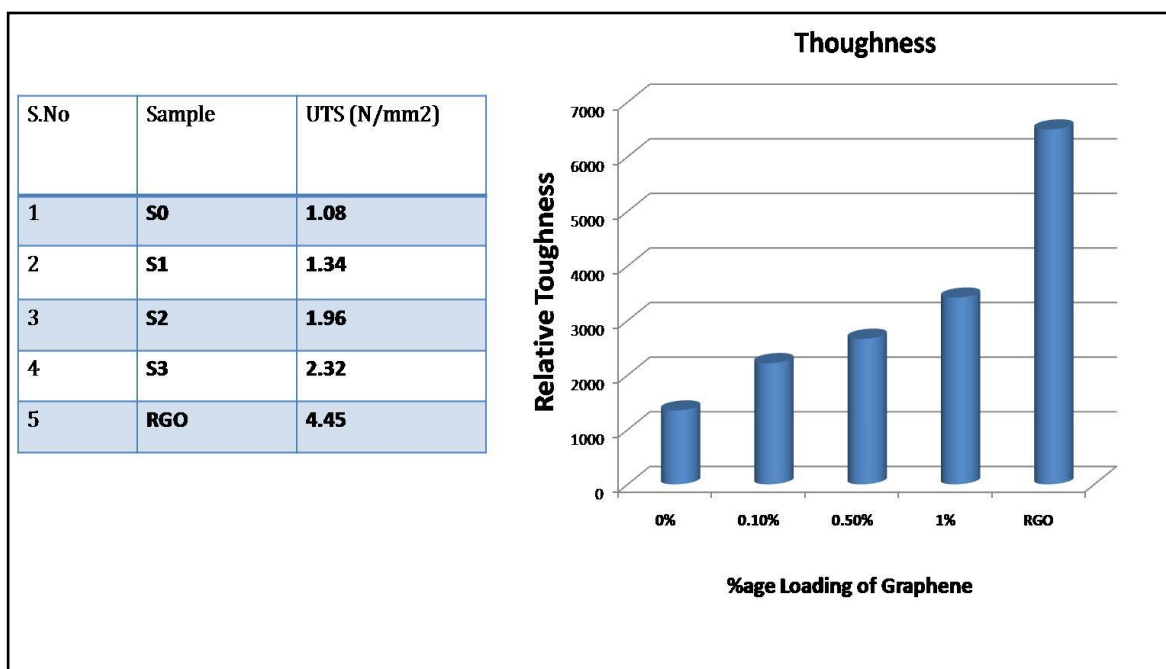


Figure 1.20 Bar graph of relative toughness for Co-composites and RGO samples

7.6.3 Flexural Stregth

Biaxial flexural strength is plotted for each sample as shown in figure 7.22. The trend remains the same as UTS, explained above from the stress - strain curve. We have 10.28 MPa for pure cobalt ferrites which is improved up to 19.92 MPa for only 1 % loading of graphene, while for RGO is so high up to 32.17 MPa.

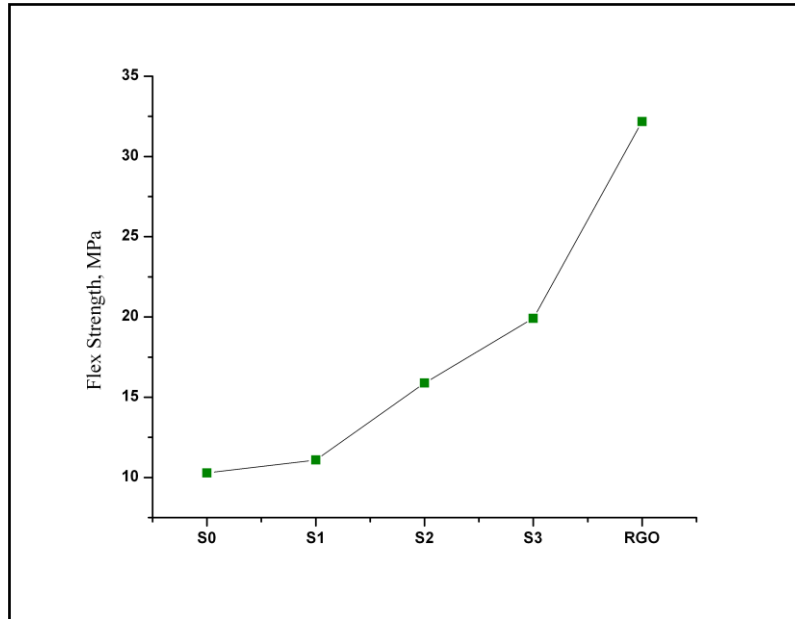


Figure 7.21 graph of flexural strength for all Co-ferrites and RGO samples on ring pellets

7.6.4 Vickers Hardness

The micro Vickers hardness test was performed on sintered pellets of composites, according to ASTM slandered C 1327 – 03[23]. Micro indents were applied to a load of 0.5 kg for 5 sec. five indents were made on each pellet. For reliable results the diagonal measurements were performed by JEOL SEM. Vickers Hardness no (Hv) were calculated by the formula [24],

$$HV=1.8544 (P/d^2)$$

Where

P = load in kgf, and

D = average length of the two diagonals of the indentation in mm.

Figure 7.23, shows that the Hv No lowered with increasing graphene loading.

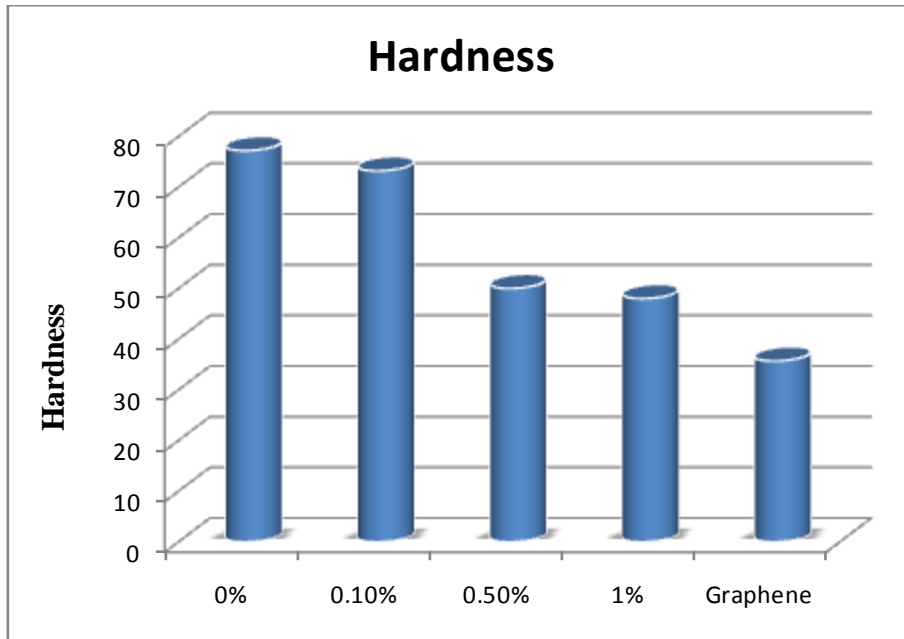


Figure 7.22 Bar graph of Vickers hardness for all samples

Cobalt ferrites have Hv.No up to 77, which decreased up to 48 for 0.5 % loading .This decrease in hardness is due to the incorporation of flexible sheets of graphene, which promote the penetration and slipping of cobalt ferrite particles under the applied load by indent. Further on graphene loading beyond 0.5 % negligible decrease in hardness reveal that after some optimum limit the graphene loading will act as a reinforcing agent in cobalt ferrite matrix and may increase its hardness.

References

1. J. S. Lukesh. Anomalous X-Ray Diffraction Spectra in Graphite. *J. Chem. Phys* 1951; 19: 1203.
2. D. C. Marcano. et al. Improved synthesis of graphene oxide. *ACS Nano* 2010; 4: 4806–4814.
3. H. Y. Jeong, et al. Graphene Oxide Thin films for flexible nonvolatile memory applications. *Nano Lett.* 2011; 10: 4381–4386.
4. Si Y, Samulski ET. Synthesis of water soluble graphene. *Nano Lett* 2008; 8: 1679–1682.
5. Zi. Z. Synthesis and magnetic properties of CoFe₂O₄ ferrite nanoparticles. *J. Magn. Mater.* 2009; 9: 1251-1255.
6. Rajendran, M., Magnetic properties of nanocrystalline CoFe₂O₄ powders prepared at room temperature: variation with crystallite size. *J. Magn. Mater.* 2001; 232: 71-83.
7. Zhang T, Zhang D, Shen MA. Low-cost method for preliminary separation of reduced graphene oxide nanosheet. *J Mater Lett* 2009; 63: 2051-2054.
8. Si Y, Samulski ETal. Synthesis of water soluble graphene. *J Nano Lett* 2008; 8: 1679-1682.
9. Stankovich . S. et al. Synthesis of graphene-based nanosheet via chemical reduction of exfoliated graphite oxide. *Carbon* 2007; 45:1558–1565
10. N. Sanpo, James Wang and Christopher C. Berndt Influence of Chelating Agents on the Microstructure and Antibacterial Property of Cobalt Ferrite Nanopowders .*Journal of the Australian Ceramic Society* 2013; 49: 84 – 91.
11. Zi, Z. Synthesis and magnetic properties of CoFe₂O₄ ferrite nanoparticles. *J. Magn. Mater.* 2009; 321:1251-1255.
12. Beny-Bassez and C Rouzaud J. N. Characterization of carbonaceous materials by correlated electron and optical microscopy and Raman micro spectroscopy. *Scanning Electron Microscopy* 1985; 1: 119-132.
13. Dresselhaus. M. S. and Dresselhaus, G. 1982. Light scattering in graphite intercalation compounds. In: *Light scattering in solids* (edited by Cardona, M. & Guntherodth, G.). Springer, New York, 3-57.
14. Tuinstra, F. Koenig, J. L. Raman Spectrum of Graphite. *Journal of Chemical Physics* 1970; 53: 1126-1130.
15. Wopenka, B. and Pasteris, J. D. Structural characterization of kerogens to granulite-facies graphite; applicability of Raman microprobe spectroscopy. *American Mineralogist* 1993; 78: 533-557.
16. Xin. GO, H. W, Kim, N, Cho and SM, Chae. H: A graphene sheet exfoliated with microwave irradiation and interlinked by carbon nanotubes for high-performance transparent flexible electrodes. *Nanotechnology* 2010; 21:1–7.
17. Rao, CNR, Sood, AK, Subrahmanyam and KS, Govindaraj. A: Graphene: the new two-dimensional nanomaterial. *Angew Chem Int Ed* 2009; 48: 7752–7777.
18. J. C. Maxwell. A Dynamical Theory of the Electromagnetic Field. *Philosophical Transactions of the Royal Society of London* 1865; 155: 459-512.
19. B. V. Hamon. Maxwell-Wagner Loss and Absorption Currents in Dielectrics. *Aust. J. Phys.*, Polarization 1953; 6304.
20. Peter Y. Yu, Manuel Cardona (2001). *Fundamentals of Semiconductors: Physics and Materials Properties*. Berlin: Springer. p. 261. ISBN 3-540-25470-6

21. H. T. Feng, R. F. Zhuo, J. T. Chen, D. Yan, J. J. Feng, H. J. Li, S. Cheng, Z. G. Wu, J. Wang and P. X. Yan. Synthesis, Characterization, and Microwave Absorption Property of the SnO₂Nanowire/Paraffin Composites Received. To the authors 2009 *Nanoscale Res Lett* 2009; 4:1452–1457.
22. Y.S. Dedkov and M. Fonin. Electronic and magnetic properties of the Graphene-ferromagnet interface. *New J. Phys* 2010.
23. ASTM F394. Standard test method for biaxial flexural strength of ceramic substrates, American Society for Testing Materials (ASTM.org), Philadelphia, PA, 1991
24. Hegazy, A.A. Thermal Joint Conductance of Conforming Rough Surfaces: Effect of Surface Microhardness Variation. Ph.D. Thesis, University of Waterloo, Canada 1985.

CHAPTER 8

Conclusion and Recommendations

8.1 Conclusion

1. New efficient chemical route for GO synthesis is studied. This new route is very useful for mono layer GO, especially for composites and sensor applications, where we need highest surface area and good adhesion with matrix or other species.
2. We successfully synthesized ribbon like structure of graphene, well dispersed on expanded sheets, may be efficient to be use in lithium ion batteries.
- 3.Reduction of GO with sodium hydroxide in this work led to environment friendly synthesis of graphene based composites with out using hydrazine, in future may be applied with other salts also.
4. We revealed that both the electrical properties and conductivity of cobalt ferrites is improved by imbedding very small amount of graphene nanosheet. Along with improving mechanical properties the graphene also widened the microwave absorption band. So it is concluded that graphene based ferrites composites may play a vital role for microwave shielding applications.

8.2 Future Recommendations

1. To increase the graphene loading to some higher concentration with in the ferrite matrix and see the effect on electrical and mechanical properties.
2. It is also possible to fabricate a flexible sheet of GO-ferrites composites which may be very efficient for light weight microwave absorbers.